NASA TECHNICAL NOTE

NASA TN D-8300

STRUCTURAL ANALYSES FOR THE MODIFICATION AND VERIFICATION OF THE VIKING AEROSHELL

Wendell B. Stephens and Melvin S. Anderson

Langley Research Center
Hampton, Va. 23665

NATIONAL AERONAUTICS AND SPACE ADMINISTRATION • WASHINGTON, D. C. • NOVEMBER 1976

1. Report No.	2. Government Accession No.	3. Recipient's Catalog No.
NASA TN D-8300		

4. Title and Subtitle
STRUCTURAL ANALYSES FOR THE MODIFICATION AND VERIFICATION OF THE VIKING AEROSHELL

5. Report Date
November 1976

6. Performing Organization Code

7. Author(s)
Wendell B. Stephens and Melvin S. Anderson

8. Performing Organization Report No.
L-10751

9. Performing Organization Name and Address
NASA Langley Research Center
Hampton, VA 23665

10. Work Unit No.
506-17-25-01

11. Contract or Grant No.

12. Sponsoring Agency Name and Address
National Aeronautics and Space Administration
Washington, DC 20546

13. Type of Report and Period Covered
Technical Note

14. Sponsoring Agency Code

15. Supplementary Notes

16. Abstract

The Viking aeroshell is an extremely lightweight flexible shell structure that has undergone thorough buckling analyses in the course of its development. In this paper the analytical tools and modeling technique required to reveal the structural behavior are presented. Significant results are given which illustrate the complex failure modes not usually observed in simple models and analyses. Both shell-of-revolution analysis for the pressure loads and thermal loads during entry and a general shell analysis for concentrated tank loads during launch were used. In many cases fixes or alterations to the structure were required, and the role of the analytical results in determining these modifications is indicated.

17. Key Words (Suggested by Author(s))
Branched shell
Buckling analysis
Experimental aeroshell verification
Mechanical and thermal loading
Viking aeroshell

18. Distribution Statement
Unclassified – Unlimited

Subject Category 39

19. Security Classif. (of this report)	20. Security Classif. (of this page)	21. No. of Pages	22. Price*
Unclassified	Unclassified	52	$4.25

*For sale by the National Technical Information Service, Springfield, Virginia 22161

STRUCTURAL ANALYSES FOR THE MODIFICATION AND VERIFICATION OF THE VIKING AEROSHELL

Wendell B. Stephens and Melvin S. Anderson
Langley Research Center

SUMMARY

The Viking aeroshell is an extremely lightweight flexible shell structure that has undergone thorough buckling analyses in the course of its development. In this paper the analytical tools and modeling technique required to reveal the structural behavior are presented. Significant results are given which illustrate the complex failure modes not usually observed in simple models and analyses. Both shell-of-revolution analysis for the pressure loads and thermal loads during entry and a general shell analysis for concentrated tank loads during launch were used. In many cases fixes or alterations to the structure were required, and the role of the analytical results in determining these modifications is indicated.

INTRODUCTION

The aeroshell component of the Viking lander capsule which enters the Martian atmosphere is shown in figure 1. The function of the conical aeroshell is to act as a decelerator upon entry into the Martian atmosphere. Since loads are relatively small and the aeroshell was optimally designed with respect to weight, it is a very lightweight flexible structure that is subject to instability failure.

The initial design took advantage of a number of previous studies (refs. 1 to 13). The circumferential reinforcements and skin thicknesses of the aeroshell were sized assuming conventional ring theory and neglecting any flexibility in the resulting reinforcement. In addition, the design was based only upon the entry load conditions, and simple analytical checks were made for dynamic and thermal effects which at that time were assumed small. As the mission environment became better defined, other loading conditions were identified that required additional analytical and experimental studies and in some cases design changes. The purpose of this report is to document the analytical studies and the associated mathematical modeling which are required for proper representation of the complex failure modes occurring in the structure. A further purpose of the report is to record the impact that these studies have had on the final design of the

aeroshell. The experimental studies were performed by the contractor, and descriptions of the tests and results are contained in references 14 and 15.

It has been shown in previous studies (refs. 1 and 2) that optimally designed structures often exhibit complex failure modes which involve the interaction of conventional modes of failure. In order to provide an adequate description of the modes of failure occurring in the flight aeroshell, a two-level analytical approach to the aeroshell structure was often required. First, an analysis was made of the overall structure to determine the general modes of failure and the corresponding critical regions of the structure. Second, a more refined analysis was made with the critical regions modeled in much greater detail in order to determine a more accurate prediction of the true strength capability for the aeroshell.

This report is presented in four sections. The first section contains descriptions of the aeroshell and the analysis procedures used for the various load conditions. The second section deals with the entry load verification and test article results. The analytical approach used is based on a one-dimensional shell-of-revolution analysis, and both collapse and bifurcation buckling are considered. Most of the modifications to the initial aeroshell were required to satisfy the entry-load condition and are presented in this section. The third section deals primarily with the analyses and tests performed for the launch load case. Due to the structural asymmetries in the support conditions and the highly concentrated loads applied by the deorbit fuel tanks, a general two-dimensional analysis was required. The fourth section describes a contingency design which would account for the pogo loading. The design procedure as well as the analysis is presented.

DESCRIPTION OF THE AEROSHELL AND ANALYSIS PROGRAMS

The Viking Aeroshell

The Viking aeroshell is shown in figure 2 and is basically a blunt biconic structure. The monocoque spherical cap is connected to an inner cone structure which is reinforced with nine lightweight Z-rings. The juncture of the cap and cone is reinforced by a T-ring. The inner cone is attached to the outer cone at the payload ring juncture. The outer cone is reinforced by an additional 18 Z-rings, and the outer edge of the cone is supported by a large closed-section base ring. (The numerous circular holes in the face of the base ring are for weight-saving purposes (fig. 2).) The payload mass is to be attached to the payload ring base at the three main support points located 120° apart and by the six shear connection points located at 33° to either side of the main supports. All of these components are constructed of aluminum. The outer skin surface of the aeroshell is coated with an ablation material approximately 0.86 cm thick. The material properties for the metal components and the ablation material are given in the following table:

Property	Shell skin	Z-ring	Ablation surface
Modulus of elasticity, E, GN/m^2	73.77	72.39	0.0152 to 0.0274
Poisson's ratio, ν	.34	.32	.5

A detailed view of a typical cross section of the aeroshell is shown in figure 3.

The conical portions of the aeroshell skin are fabricated from 120^{o} segments which were chem-milled to the different thicknesses as required. The portholes, windows, inclusions, and splice seams of the aeroshell shown in figure 2 are ignored in the analysis since the reinforcements around these structural changes were designed so that they would not decrease the strength of the shell.

Analysis Programs

Since the structural reinforcements around the cutouts and inclusions tend to preserve the rotational symmetry of the stiffness, extensive use was made of advanced, efficient, one-dimensional shell-of-revolution codes for much of the analytical work, particularly for correlation with the uniform pressure tests performed on the structure. The use of a shell-of-revolution code, however, further implies that the boundary constraint along the payload attachment flange must be assumed continuous rather than having the three discrete rigid attachments and six shear pin connections discussed earlier. A study of the effect of this assumption was made in reference 9 and was shown to have little influence on buckling strength for pressure load cases. As shown in reference 9, the entry loads are reacted at discrete points along the base of the payload ring and are redistributed into a fairly uniform meridional internal load at the top (juncture) of the payload ring at the conical surface. Although many shell-of-revolution codes are capable of analyzing this structure, notably those described in references 16 to 18, the SRA (Structures Research Associates) computer program (ref. 18) was chosen since it includes the capability for modeling shell branches and could, if necessary, be used to ascertain the degree of sensitivity of the structure to small initial geometric imperfections.

The launch condition introduces concentrated loads from the fuel tanks directly to the shell surface structure and therefore causes asymmetric stress fields. For these stress conditions a general two-dimensional shell-analysis tool must be used. One of the most accurate and numerically efficient programs that account for this type of response is the two-dimensional finite-difference STAGS (Structural Analysis of General Shells) code described in reference 19.

The following sketches indicate the locations of the discrete reactions R as well as the inertial loadings for the launch and entry flight conditions. The reactions are located circumferentially at the three main support points and at the six shear pin points:

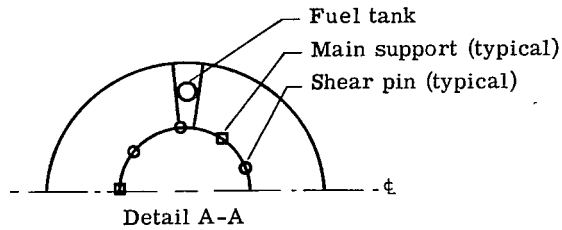

Detail A-A

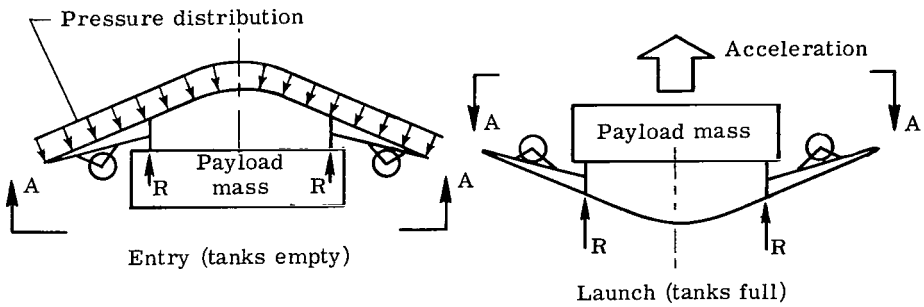

STRUCTURAL ANALYSIS OF TEST ARTICLES FOR ENTRY LOAD VERIFICATION

In this section analyses and results of tests performed to qualify the aeroshell for the entry condition are presented. Also, several design changes resulting from these studies are described. Prior to aeroshell fabrication a similar prototype aeroshell (ref. 9) had been fabricated and tested which served as a guide in the flight aeroshell development.

Description of the SRA Model

Prior to the first static uniform pressure test on the proposed aeroshell a critical analytical evaluation of the buckling strength was made using the shell-of-revolution code. The shell was modeled as a rotationally symmetrical structure having the profile shown in figure 3 with the exception that the thickness change from 0.089 cm to 0.170 cm occurred at a radius of 73.4 cm rather than 61.0 cm. More detailed dimensions showing ring attachment locations and properties are given in reference 1. The 27 small Z-rings were modeled initially as discrete rings with the conventional assumption that the ring cross sections would remain rigid. The payload and base rings, however, were each modeled as shell structure.

Analysis of Baseline Aeroshell

Using this model of the baseline aeroshell two types of analyses were performed. First, a bifurcation buckling analysis based on a linear axisymmetric prebuckling state was performed yielding a critical buckling load corresponding to a pressure of 34.5 kN/m^2 and a mode shape which included five full circumferential waves (n = 5) in the outer cone portion of the aeroshell. Other near-critical modes existed which included local buckling modes where some rings in the inner cone would move with the buckle and some would behave as nodes. Second, an axisymmetric (n = 0) nonlinear collapse analysis was performed showing a collapse pressure of 24.1 kN/m^2 with the largest deflection occurring in the highly stressed region in the vicinity of the payload ring.

First Modification and Test of the Aeroshell

After comparing the preceding results with the prototype studies in reference 9 and observing that the region of the prototype surface where the payload was attached was reinforced with stringers, it was decided to strengthen the inner cone skin by allowing the 1.70-mm skin to extend inboard to a radius of 61 cm. This strengthening would suppress much of the local buckling behavior as well as relieve any concern that geometric imperfections would interact with the axisymmetric prebuckling deformations to cause premature failure. This extension inboard of the 1.70-mm-thick skin to a radius of 61 cm was the first modification required to strengthen the shell. The aeroshell with this modification is referred to hereinafter as the aeroshell with modification 1. This modification had negligible effect on the calculated bifurcation buckling load but increased the nonlinear collapse load to a pressure corresponding to 34.3 kN/m^2 as shown in figure 4 where the buckling load is plotted as a function of harmonic behavior.

An aeroshell with modification 1 was tested, and the test result is also shown in figure 4. The shell buckled in six harmonics in the outer cone at a pressure of 13.2 kN/m^2 which was far below the predicted buckling pressure of 34.5 kN/m^2 and well below the required load corresponding to a pressure of 17.5 kN/m^2. Experience with the prototype structure (ref. 9) had shown that correlation factors of experiment to analysis of approximately 0.7 could be expected. For this case the correlation (knockdown) factor is 0.38, indicating additional effects were influencing the test result. A study of strain-gage data showed that the outstanding flanges of the Z-ring reinforcements had not carried any appreciable load during the test but instead had rolled laterally, leaving the skin only lightly reinforced. These rings were far more flexible than conventionally designed rings due to the optimal design of the structure.

A reanalysis of the structure was performed modeling the Z-ring webs and the T-ring web at the cap-cone juncture as portions or as branches of the shell structure. The flanges of the Z-rings were modeled discretely. As shown in figure 4, the predicted

critical pressure for this model is now 17.0 kN/m^2 with a general buckling mode in the outer cone at $n = 7$. The notation "branched" or "discrete" in the figure refers to the type of model used to represent the small reinforcing Z- and T-rings. The resulting correlation of test with analysis is now 0.78, which is within the expected accuracy for such studies. In addition, the stress analysis showed that the outstanding flanges of the Z-rings were virtually unstressed, as was observed in the experiment. The axisymmetric collapse load was essentially unaffected by this model change since the maximum deformations for this type of failure occur inboard of the payload ring.

Second Modification and Test of the Aeroshell

The test and improved analysis of the aeroshell with modification 1 indicated that the structure still needed to be strengthened to reach the critical design pressure of 17.5 kN/m^2 for entry to the Martian atmosphere. Since replacement or refabrication of the rings was deemed too costly, a method of reinforcing the existing design was sought. Since the rolling distortion of the rings appeared to be the primary cause of the low buckling load, a modification was made which tied the rings to the skin and tended to preserve the angle between them. Small triangular clips were riveted to webs of the Z-rings and to the skin surface. The clips were located about every 12.7 cm along the ring circumference. The aeroshell with both this modification and modification 1 is referred to hereinafter as the aeroshell with modification 2.

The clips could never be modeled accurately by the shell-of-revolution code since they represent meridional (stringer) reinforcement and can only be accounted for as "smeared" reinforcement on the webs of the Z-rings. An attempt was made to measure the clip effectivity by varying the clip elasticity modulus. Essentially, the procedure was to plot the calculated Z-ring outer flange stress resultant and the aeroshell buckling strength each as a function of the clip modulus. During the test the stress level in the critical flanges was monitored (through strain-gage data) allowing estimates of clip effectivity and buckling strength to be made. Using this approach it was determined that the modified modulus of the clip material in the analysis should be 0.5 percent of the original modulus. The analytical buckling strength is shown in figure 5 as a function of the circumferential wave number. The analytical buckling strength effectivity increased from a pressure of 17.0 kN/m^2 at $n = 7$ (modification 1) to a pressure of 25.4 kN/m^2 at $n = 6$ (modification 2). The collapse strength increased from a pressure of 34.5 kN/m^2 to 39.6 kN/m^2 and is also shown in figure 5.

Experimentally the clip-reinforced aeroshell failed catastrophically at a pressure of 16.1 kN/m^2 in the axisymmetrical mode ($n = 0$) in the inner cone and cap while simultaneously reaching incipient buckling in the outer cone in the $n = 6$ mode. The loading

and support condition were identical to those used in the previous test. The attachment flange of the payload ring failed (fractured) and consequently precipitated the inner-cone collapse. Since the ring fractured and since $n = 6$ failure was imminent, the test result is represented in figure 5 at $n = 6$. The correlation factor between experiment and theory is 0.65. This correlation is poor compared with the excellent results which were published in reference 9 and the earlier value of 0.78 for the unclipped shell. This poor correlation is due in part to the fracture of payload ring attachment flange and the fact that the general $n = 6$ buckling mode never fully developed. It was hypothesized that the failure of the inner-cone attachment flange of the payload ring was due to the high bending stresses from the payload reaction at the juncture. These stresses were increased by the eccentric load path in the skin profile at the payload ring juncture (see fig. 3). The eccentricity of this load path was not included in the analytical model, however, and the high stresses were not predicted prior to the test. Also, the poor correlation is attributed in part to a poor "calibration" of the clip effectivity. The low effective modulus required to correlate the stress results with experiment indicates that this is not a very satisfactory procedure for describing the actual behavior. Also, the discreteness effect of the clips on buckling strength is probably much more severe for the higher ($n \geq 2$) harmonic buckling cases than for the axisymmetric stress state initiating buckling.

Third Modification of the Aeroshell

A number of modifications to the aeroshell were made following the test of the aeroshell with modification 2 and are shown in figure 6. First, an additional channel ring was placed at a radius of 25.25 cm in the spherical cap region to assure that the stresses being transmitted from the cone to the cap were not excessive near the juncture of cap-cone interface. Second, a circumferential splice plate was added at the payload ring juncture which removed the eccentric load path and served to reduce the high stress levels caused by the payload reaction introduction in this region. Third, the number of clips in the inner cone was doubled, and the number of clips around cutouts, portholes, etc. in the outer cone was increased. Also, all clip-free edges were flanged to increase the clip rigidity. Finally, the entry corridor for the Viking flight was modified so that the new ultimate design load could be taken as a pressure of 15.6 kN/m^2. The aeroshell with these modifications as well as the previous ones is referred to hereinafter as the aeroshell with modification 3. These additional structural modifications, which are shown in figure 6, have little effect on the calculated buckling strength but do reduce the excessively high stresses at the payload ring juncture and improve the rigidity (stiffness) of the Z-rings on the real structure. Three flight aeroshells which included all of these modifications were subsequently prooftested to a pressure of 13.7 kN/m^2 without any indications of failure. The analytical results for the aeroshell with modification 3 are shown in figure 5.

The analytical mode shapes corresponding to the minimum buckling values shown in figure 5 are presented in figures 7(a), 7(b), and 7(c) for the various branched aeroshell models. The mode shapes are superimposed on the undeformed aeroshell profile.

Effect of Thermal Loads on Buckling Strength

The effect on aeroshell buckling strength of two thermal load conditions which occur during entry was also studied. First, the effect of the temperature occurring at peak dynamic pressure was evaluated. The expected temperature profile along the skin surface for this case is shown in figure 8 where the solid curve represents the predicted temperatures, the dashed curve represents the ultimate temperatures, and the dot-dashed curve represents the temperatures modeled in the analysis. This temperature profile is the one estimated to be present at maximum dynamic pressure. These temperatures deviate very little from the initial assumed entry temperature of 21° C, and in the early stages of design the effect of these deviations was neglected. The thermal drop in temperature along the aeroshell meridian at 80.0 cm and greater than 170 cm is due to the mass of the payload and base rings. For this case the T- and Z-rings are assumed to be the same temperature as the skin, and the base of the payload ring support is expected to drop to a temperature of 21° C. Thus, the largest thermal gradient occurs in the payload ring juncture region.

A second thermal load condition which corresponds to the predicted maximum temperature case was studied. At this time in the entry flight the pressure loads are small enough to be neglected. The temperature profile for this case is presented in figure 9 where the dot-dashed curve again represents the loads modeled in the analysis and where the influence of concentrated masses at the cap-cone, payload ring, and base ring junctures on the temperature profile is indicated by sharply lower temperatures. The free edge of the reinforcing rings is assumed to have a temperature drop from the skin temperature varying linearly from 3° C at ring 1 to 9° C at ring 27. The payload ring temperature drops to 20° C along the payload attachment flange.

The effect of the thermal loads at maximum dynamic pressure on buckling strength is shown in the load interaction curves in figure 10. Here buckling strength due to a uniform pressure is plotted along the ordinate, and the factor multiplying the thermal load state represented in figure 8 is plotted along the abscissa. Both local buckling and general buckling estimates of strength are shown in the figure. The local buckling estimates fall below the general buckling curve, and there is a loss of strength in the local buckling strength estimates as temperature increases; however, the general buckling modes are sensitive to initial imperfections. For this reason the factor for correlating experiment to analysis is applied to general buckling results and this corrected general buckling curve governs. The results show that a correlation factor as low as 0.63 is acceptable, and the tests have already shown the correlation factor to be in excess of 0.69. The general

buckling estimates (low n number) show an insensitivity to the presence of the low temperatures. In fact, a small increase in buckling strength occurs as temperature factor increases. The numerical integration scheme used in the SRA program (ref. 18) failed to converge with the available computer core storage for higher harmonic (n number) calculations; therefore, estimates of local buckling strength were made using results from the axisymmetric biaxial stress state and assuming that buckling which occurs between Z-rings is equivalent to simply supported plates. The stresses in each Z-ring bay were averaged.

The heat shield which covers the outer surface of the aeroshell was assumed to have no contribution to structural strength so an added degree of conservatism exists in the combined low-temperature state – maximum dynamic pressure buckling strength calculations. If a uniform layer of ablation material 0.43 cm thick with a modulus of 27.4 MN/m^2 remains on the aeroshell outer surface at the time of maximum dynamic pressure, the increase in buckling strength is approximately 9 percent as shown in figure 11. The solid curve for the analysis of the aeroshell with only the pressure load is added for reference.

For the second thermal load case where there are maximum temperatures and gradients (defined in fig. 8) and very low pressures (assumed to be zero in the analysis) the computed general buckling load is several times the applied load. The local buckling (high n number) was found to be the governing failure mode of the shell at these temperatures. The calculation of local buckling, based on the simple supported flat-plate procedure using the axisymmetric stress-state results from the complete aeroshell model, yielded a failure between Z-rings 10 and 11 at 95 percent of the applied load. (Rings 10 and 11 are the first two Z-rings outboard of the payload ring.) A more accurate analysis was then undertaken with a model which included the critical bay (between rings 10 and 11) along with the two adjacent bays. Results from the axisymmetric stress analysis for the complete shell were used to obtain the boundary conditions and stress state of the smaller model. This procedure was used to make a detailed local buckling study of the critical region which would include the effects of nonuniform stresses, deformations, thickness change in the skin, and flexibility of the Z-rings by modeling them as part of the shell. Results from this more accurate analysis showed the buckle strength was 1.59 times the applied thermal state at n = 65. This result is shown in figure 12.

The resulting mode shape at n = 65 is superimposed on the undeformed surface in figure 13. The attachment of the Z-ring to the shell skin is located approximately at the center of the attachment flange. The mode shape shows that the Z-ring is quite flexible and that there is some relative motion between the Z-ring flange and the shell skin. Ring 10 is twice as thick as ring 11, and therefore ring 11 shows more displacement in this modal plot. The Z-rings are stiffer than freely rotating simply supported edges assumed in the flat-plate procedure, and this increased stiffness along with inclusion of

shell curvatures and prebuckling deformation caused the local buckling-strength estimate to increase from 0.95 to 1.59 times the applied thermal loads.

The differences in buckling behavior between the uniform pressure, the low-temperature pressure, and the maximum temperature cases can be better understood by examining the compressive circumferential stress resultants in the outer cone of the aeroshell where the buckling is expected to occur, as shown in figure 14. The differences in the stress distributions of the uniform pressure case and the uniform pressure combined with low thermal loads case are slight and account for the almost linear behavior of the interaction curve for general buckling shown in figure 10. The maximum temperature stress resultant distribution, however, is radically different from these cases. The only significant compressive stress for this case occurs near the payload ring and base ring attachments, and these stresses cause the local buckling behavior to govern. The high compressive stress and the corresponding local buckling occur between Z-rings 10 and 11.

Higher-Order Effects

In general, the shell-of-revolution analyses are based on stress states which are linear and axisymmetric and which include meridional rotations. A brief study was made to assess the importance of including rotations as well as the necessity of using nonlinear analysis. The results of the study are shown in figure 15 where buckling strength is plotted as a function of the circumferential wave number. The loading is again the uniform normal pressure. The solid curve shows the results for the linear prebuckling analysis with rotations included. The buckling strength based on nonlinear stress states which include rotations shows a 5-percent increase in strength, and the buckling strength based on linear stress states without rotations showed a 7-percent increase in strength. For buckling due to uniform pressure these effects are small, and the linear prebuckling state with rotations included appears to be conservative.

STRUCTURAL ANALYSIS OF TEST ARTICLES FOR LAUNCH LOAD VERIFICATION

Description of Launch Loads

Qualification flight tests showed much higher loads than expected during launch due to the presence of pulsating dynamic loads (pogo); therefore, these loads had to be examined to determine if they were critical in terms of the buckling strength of the aeroshell. Both experimental and analytical studies were made (refs. 14 and 15).

At launch, the aeroshell resides in the flight vehicle in an inverted (apex pointing toward Earth) position such that the two spherical deorbit fuel tanks shown in figure 16

apply nearly concentrated loads to the structure. The shell structural masses all undergo a heavy g loading at a time when the deorbit fuel tanks are fully loaded. The tanks are connected to the aeroshell as shown in figure 16 and introduce the nearly concentrated loads into the aeroshell base and payload rings through the tank support trusses. The trusses are attached to the payload ring and base rings at four points (fig. 16(b)) for each of the two deorbit fuel tanks. The tank reactions are statically determinate due to pin connections with radial slots at the base ring attachments and pin connections at the payload ring attachments. In the launch configuration the loading reacts on the aeroshell in such a manner that it attempts to push the outer cone of the shell inside out.

Description of STAGS Model

The concentrated loads introduced through the tank trusses represent a load condition which cannot be accurately represented by a one-dimensional shell-of-revolution code. The two-dimensional STAGS program for general shell analysis was used, therefore, to obtain the bifurcation buckling strength based on a linear stress state.

A general shell code must be used to model properly the discrete lander attachments on the payload ring represented by the three rigid support points, and six shear connections can be modeled in detail. In addition, the STAGS code has a feature which is particularly suitable for the manner in which launch loads were applied during tests. The loads which caused bifurcation buckling can be separated into two parts: a steady-state or constant load which is not a function of the eigenvalue and loads which are functions of the eigenvalue. The value of the tank load (either hydraulically or dynamically applied during the tests) is the parameter which is varied during the test, and the remaining inertial loads are held constant. This load system can be duplicated directly in the STAGS analysis.

The STAGS analytical model, loads, and support conditions are fully described in the appendix. Briefly, the model is composed of the cap, inner-cone and outer-cone segments, and the webs of the payload ring and the first four Z-rings in the outer cone modeled as an aeroshell structure. The remaining Z-rings are treated as smeared stiffeners. Also, the rings at the cap inner cone and the payload ring junctures and the base rings on the outer cone and the payload web are all modeled discretely. From preliminary analysis using simple STAGS models it was found that the significant buckling was confined to the area outboard and near to the payload ring, and therefore this region had to be modeled in greater detail. The modulus of the smeared rings was reduced until the bifurcation buckling load due to a normal pressure was in agreement with the experimentally derived load. This adjustment of the smeared-ring modulus was made to account for the flexibility of Z-ring stiffeners and Z-ring clips. Basically, the analytical model is of the baseline aeroshell with the clips and modifications accounted for in the quasi-empirical manner of adjusting the smeared-ring modulus. The ring modulus selected was 18.3 percent of the

skin modulus. Using the plane of symmetry shown in figure 16(b), which passes through the aeroshell axis and the main support point on the payload ring that is furthest from (and equally distant from) the two deorbit fuel tanks, requires that only one half of the aeroshell needs to be modeled. The model is more completely described in the appendix. In this 180° model the main supports along the payload ring base are located at 60° and 180°, and the tank truss supports are symmetrically located about the 90° meridian at both the payload ring-cone juncture and the base ring-cone juncture.

Launch Load Analysis and Test Results

An interaction curve based on linear bifurcation buckling analysis for the g loads (excluding the tank loads) versus the tank load is presented in figure 17. Three sets of test data are presented along with the analytical results. Tests 1 and 2 were performed on an aeroshell test article with modification 1. Test 3 represents results from an aeroshell with modification 3. In test 1 the tank load is represented by a static jack load hydraulically applied to the truss structure, and the inertial loads are represented by laying shot bags to the inner surface of the aeroshell. Tests 2 and 3 represent results in which the tank loads were applied dynamically and inertial loads were applied through air bags. The solid symbols represent the loads at which incipient buckling (first observed strain reversal) occurred during the test. The loading of the structure continued until collapse was believed imminent, which is presented by the open symbols.

The tank load reactions at the base ring apply meridional compression to the structure while the tank load reactions at the payload ring hardly affect the stress behavior of the aeroshell skin. The analytical buckling failures in which tank loads dominate were generally quite localized outboard of the payload ring and close to the 80° meridian where the local meridional stresses caused buckling under these load conditions. The inertial loads add meridional compression also. The dashed curve in figure 17 represents the initial calculations which were far below experimental values. For these calculations the heat-shield material, which has a very low modulus of elasticity, was neglected. This material has a modulus in a range of 15.2 to 27.4 MN/m^2. At launch, however, the virgin ablation material has a nominal thickness of 0.86 cm, and this material adds significant bending stiffness to the structure. The test articles had the ablation material on the structure so that a uniform outer layer with the 0.86-cm thickness was included in the analytical model. The analytical buckling strength with the heat-shield material added was then found to be in close agreement with test results as shown in figure 17. The cross-hatched region at the left shows where local buckling is expected to occur for the range of values for the modulus of elasticity of heat-shield material studied. A study was then made to determine the effect of suppressing the local buckling. The skin and Z-ring web material in the locally buckled region near the payload ring and tank truss supports were strengthened by adding 0.081-cm-thick doublers. With this local reinforcement, the analytical mode

was found to be a general shell mode in the outer-cone region with a 35-percent increase in buckling strength. Thus, the cross-hatched region at the right shows where general buckling would occur if local buckling could be suppressed or is not catastrophic.

For test 1 at 0.78g, buckling was judged to be imminent and excellent agreement with theory is obtained. The tank loads for test 2 at 4.56g show excellent agreement with local and general buckling predictions. Test 3 demonstrates that the flight article (modification 3) strength is higher than predicted. This difference is attributed to the presence of the flanged clips, splice plate, and channel-ring modification which are not included in the structural analytical model.

Typical analytical contour plots for meridional stress resultants on the developed surface of the aeroshell due to both the g (inertial) loads and a unit tank load are shown in figures 18(a) and 18(b), respectively. For the 1g load the outer cone is in compression with peak stresses occurring near the main support points at 60° and 180° along the payload ring interface. The inner cone is in tension. For the unit tank load, the maximum compression occurs around the 90° meridian and again outboard to the payload ring juncture. The buckle mode shape for normal displacement is shown in figure 19 and highlights the local character of the buckling due to the high stresses caused by the tank load at a value of 4.30 kN. The tank load in this case was canted 20° to account for lateral inertia effects.

It was shown in reference 1 that the structure would be sensitive to imperfections for the entry load conditions. For the launch load conditions, however, the sensitivity of the structure to small initial geometric imperfections was studied using the SRA model (with line loads applied in lieu of concentrated loads) and indicated that these imperfections would not adversely affect buckling strength.

Additional questions that arose during analyses and tests of the aeroshell were the effect of reverse loads and the effect of applying tank loads in and out of phase. The additional load required for buckling is calculated for the dynamic load which is (a) applied symmetrically, (b) applied on one tank only, (c) applied asymmetrically, and (d) applied in reverse direction. The total load on each tank is shown in figure 20. The results show the symmetric case is the most severe and the buckling load for reversed loading is about 47 percent higher than for the basic case.

CONTINGENCY DESIGN FOR INCREASED LAUNCH LOADS

Local Stiffening Approach

Contingency plans were developed to increase aeroshell strength by a factor of at least two in case modifications to suppress pogo could not be developed in time. An accumulator to suppress pogo was successfully added to the launch vehicle so that the

contingency designs were not needed. The contingency design investigated herein was a local stiffening approach. Basically, the approach was concerned with controlling the local buckling pattern, shown in figure 19, by increasing the shell stiffness in the region of the outer cone where local buckles develop. This approach involved "bonding" 0.081 cm panels to the inner surface of the skin over the relatively narrow region in which significant local buckling occurred, as shown in figure 21. The webs of rings 11 through 16 in this region were also bonded by this skin doubler material. (For this study the webs of rings 15 and 16 also had to be modeled as shell structure in the STAGS analysis.) The reinforcement is local and only needs to be placed in the two regions (180^{o} apart) where local buckling is expected. For structural modeling purposes the stiffness of the heat-shield material in this region was neglected since it was desired to have a fix that did not depend on the stiffness of the heat shield. Since it had already been determined that suppression of local buckling would only increase the load by 35 percent, additional stiffening in the outboard region was required. Four longitudinal stringers were added spanning the distance from ring 15 to the base ring and at the circumferential locations shown in figure 21. The stringer cross section is also shown. The function of the stringers is to remove completely the buckling behavior from the region in high compression due to the tank reactions on the base ring. The stringers efficiently satisfy stiffness requirements if they are spaced closely enough together so that buckling will not occur between stiffeners.

Using the modification described in figure 21, which includes both the bonded skin material and the four stringers, the analytical buckling strength from the STAGS analysis increased by a factor of 2.46 times the buckling load of the shell without the local stiffening. The meridional stress resultant distributions for this analysis are shown in figure 22(a) for the steady-state inertial loads excluding the tank load and in figure 22(b) for the unit tank load and do not differ significantly from those distributions without the local reinforcement shown in figure 18. The normal displacement buckling mode, however, presented in figure 23 differs significantly from the mode shape shown in figure 19. The buckle pattern, while still local, occurs outside the highly stressed reinforced region. The local strengthening modification would involve a mass penalty of 5.44 kg, and parallel studies showed that it could be fabricated easily and bonded onto the structure.

Evaluation of Contingency Design for Entry Loading

The locally stiffened shell was reanalyzed under the entry load design conditions to determine the effect of the local stiffening for this condition, and it was found to be minimal. The analytical buckling pressure using the STAGS models increased from 14.0 kN/m^2 to 15.1 kN/m^2 when the local stiffening was added. The analytical buckle mode shapes for

the normal displacement for the unstiffened and stiffened aeroshells are shown in figure 24. The basic seven-wave buckle pattern holds in each case except in the region where local stiffening is applied.

CONCLUDING REMARKS

The application of sophisticated advanced aeroshell analysis programs to determine the structural integrity of the Viking aeroshell has been presented. Because of the lightweight construction of the aeroshell, potential failure areas had to be carefully defined and detailed modeling in these failure areas was required. A coarse analysis model was used to identify critical failure modes and critical areas. These areas were then represented with a more refined model with much greater detail for final analysis. A one-dimensional shell-of-revolution analysis was used to determine the structural integrity under entry load conditions by including the effects of ring flexibility, temperature variations, stress concentrations around load introduction points, and geometric nonlinearities. When the small Z-rings were properly accounted for in the model, excellent agreement between tests and analysis was obtained. As a result of these analyses and the tests performed by the contractor, several aeroshell structural modifications were made. These modifications included increasing the skin thickness inboard of the payload ring juncture, adding a doubler to the inner- and outer-cone splice, stiffening the light circumferential Z-rings with clips, and reinforcing the aeroshell dome with an additional ring near the inner-cone edge. It was found that the clips reinforcing the Z-rings strengthened the shell, but this effect could not be accurately modeled. Also, it was found that the low thermal gradient at maximum dynamic pressure resulted in a slight increase in general buckling strength. Preliminary analysis at maximum temperature indicated a potential local buckling problem outboard of the payload ring; however, accurate modeling using shell theory in a subsequent analysis indicated that the design conditions were met.

The two-dimensional STAGS computer program was used to determine the structural integrity during the launch condition where large concentrated loads were applied to the aeroshell. Results indicated that the failure modes were localized and that the bending stiffness of the heat-shield material is needed to withstand the local buckling.

The stresses causing buckling due to entry loads are primarily the compressive circumferential stresses. The compressive meridional stresses cause buckling when the launch loads are applied to the structure. Imperfection sensitivity analysis shows that small initial geometric imperfections will not adversely affect buckling strength for launch load conditions and its associated local buckling phenomena. For contingency

design purposes, a lightweight means of doubling the strength of the aeroshell to withstand launch loads was determined utilizing a local-region stiffening approach.

Langley Research Center
National Aeronautics and Space Administration
Hampton, VA 23665
August 30, 1976

APPENDIX

DEFINITION OF THE STAGS MODEL, LOADS, AND SUPPORT CONDITION

The modeling detail must be reduced from that which was present in the one-dimensional shell-of-revolution analysis since a two-dimensional analysis impacts rapidly on computational storage and run times. The meridional profile presented in figure 25 highlights some of the structural detail used for the STAGS model. The major difference from the shell-of-revolution model involves the manner in which the Z-rings are represented. Since the buckling behavior can be expected to be localized near the introduction of concentrated loads, the branch modeling of the Z-rings after some preliminary analyses and study was confined to the first four ring webs outboard of the payload ring. The remaining Z-rings were all treated as "smeared" rings. The modulus of elasticity for the smeared rings, however, was reduced due to ring flexibility so the analytical model (without ablation material) would yield the bifurcation buckling strength due to a normal external pressure predicted by experiment. The additional rings which were modeled discretely included the T-ring at the cap inner-cone juncture, the T-ring and splice plate at the payload ring juncture, the channel ring at the base of the payload ring, the base ring, and the flanges of the four branched Z-rings. Longitudinal stiffeners on the branched payload ring at the rigid attachment points and the truss supports and the truss center line were modeled discretely. The stiffness properties of the discrete and smeared rings are given in table I. Associated ring locations are shown in figure 26 (and the associated skin thicknesses are shown in fig. 3). Since pole conditions are not allowed in current versions of STAGS, a small circular hole is placed at the cap pole and an artificial ring reinforced the edge. The ring is designed so that the pole condition is approximated.

The finite-difference grid in the meridional direction is indicated by the number of rows in figure 25 along with other structural model details. The finest grid spacing occurs in the outer cone where buckling is anticipated. In the circumferential direction a grid line is placed uniformly every 5°. The grid pattern excluding the cap and ring web branches is shown as a developed surface in figure 27. The heavy lines indicate junctures for the payload and Z-ring shell branches. The 1g load factors for the steady-state inertial loads are shown schematically in figure 28. The concentrated loads are due to the lander mass.

The support conditions during the launch load tests are applied to both the payload ring base and payload ring-cone juncture. At the base of the payload ring in the model the lander main supports are placed at 60° and 180° and the shear pin supports are placed at 25°, 95°, and 145° as shown in figure 28. At the latter three locations radial and circumferential displacements are assumed restrained. At the payload juncture the test article is mounted (nose cap pointing down) on three supports alined with the three main

support points of the lander. The 180° model includes only the main support at 60° and 180°. At the juncture of payload ring and outer cone, the displacements in the axial and circumferential directions are restrained at these two locations.

REFERENCES

1. Heard, Walter L., Jr.; Anderson, Melvin S.; and Stephens, Wendell B.: The Effect of Ring Distortions on Buckling of Blunt Conical Shells. NASA TN D-7853, 1975.

2. Leonard, Robert W.; Anderson, Melvin S.; and Heard, Walter L., Jr.: Design of a Mars Entry "Aeroshell." NASA paper presented at the International Symposium on Buckling of Structures (Cambridge, Mass.), June 1974.

3. Cohen, Gerald A.; Foster, Richard M.; and Schafer, Everett M.: Analysis of Conceptual Designs for the Voyager Entry Capsule. NASA CR-66580, 1968.

4. Cohen, Gerald A.; Foster, Richard M.; and Dowty, James R.: Synthesis of Optimum Structural Designs for Conical and Tension Shell Mars Entry Capsules. NASA CR-1365, 1969.

5. Cohen, Gerald A.: Structural Optimization of Sandwich and Ring-Stiffened 120 Degree Conical Shells Subjected to External Pressure. NASA CR-1424, 1969.

6. Anderson, M. S.; Fulton, R. E.; Heard, W. L., Jr.; and Walz, J. E.: Stress, Buckling, and Vibration Analysis of Shells of Revolution. Comput. & Struct., vol. 1, nos. 1/2, Aug. 1971, pp. 157-192.

7. Cohen, Gerald A.: The Effect of Edge Constraint on the Buckling of Sandwich and Ring-Stiffened 120 Degree Conical Shells Subjected to External Pressure. NASA CR-795, 1967.

8. Dixon, Sidney C.; and Carine, John B.: Preliminary Design Procedure for End Rings of Isotropic Conical Shells Loaded by External Pressure. NASA TN D-5980, 1970.

9. Heard, Walter L., Jr.; Anderson, Melvin S.; Anderson, James Kent; and Card, Michael F.: Design, Analysis, and Tests of a Structural Prototype Viking Aeroshell. J. Spacecr. & Rockets, vol. 10, no. 1, Jan. 1973, pp. 56-65.

10. Anderson, James Kent; and Davis, Randall C.: Buckling Tests of Three 4.6-Meter-Diameter Aluminum Honeycomb Sandwich Conical Shells Loaded Under External Pressure. NASA TN D-7935, 1975.

11. Anderson, James Kent; and Davis, Randall C.: Buckling Tests of Two 4.6-Meter-Diameter, Magnesium Ring-Stiffened Conical Shells Loaded Under External Pressure. NASA TN D-7303, 1973.

12. Davis Randall C.; and Cooper, P. A.: Interactive Design of Large End Rings on Stiffened Conical Shells Using Composites. Comput. & Struct., vol. 4, no. 3, May 1974, pp. 647-657.

13. Williams, J. G.; and Davis, R. C.: Buckling Experiments on Stiffened Cast-Epoxy Conical Shells. J. Exp. Mech., vol. 15, no. 9, Sept. 1975, pp. 329-338.

14. Sparhawk, H. E.; Fogg, K. L.; and Brown, H.: Viking Aeroshell Test Failure Report. VER-275, Martin-Marietta Corp., Aug. 1973.

15. Viking Program Technical Data Report – Aeroshell Dynamic Compatibility Test (POGO). TR-3720517 (Contract NAS 1-9000), Martin-Marietta Corp., Apr. 1, 1975.
Vigil, R. A.: Volume I – Text.
Payne, K. R.; and McKay, E. L.: Volume II – Test Data Tabulations [for] POGO Proof Vibration Tests.

16. Bushnell, David: Stress, Stability, and Vibration of Complex Branched Shells of Revolution: Analysis and User's Manual for BØSØR4. NASA CR-2116, 1972.

17. Svalbonas, V.: Numerical Analysis of Stiffened Shells of Revolution – Volume I of VII. NASA CR-2273, Vol. I, 1973.

18. Cohen, Gerald A.: Computer Analysis of Ring-Stiffened Shells of Revolution. NASA CR-2085, 1973.

19. Almroth, B. O.; Brogan, F. A.; Meller, E.; Zele, F.; and Petersen, H. T.: Collapse Analysis for Shells of General Shape. Volume II – User's Manual for the STAGS-A Computer Code. AFFDL-TR-71-8, U.S. Air Force, Mar. 1973. (Available from DDC as AD 762 543.)

TABLE I.- STIFFENER PROPERTIES FOR THE STAGS ANALYSIS

[See location code in fig. 26]

Location	Modulus, E, GN/m^2	Area, A, cm^2	Inertia, I_S, cm^4	Inertia, I_Z, cm^4	Inertia, I_{SZ}, cm^4	Torsional stiffness, GJ, $N\text{-}m^2$	$\bar{z}$, cm	$\bar{s}$, cm
A	72.4	0.568	1.165	1.165	0	17.11	0	0
B	72.4	.568	1.165	.499		17.11	-.579	0
C[a]	13.5	.165	.1136	0		10 062	-1.080	
D	73.8	.830	.0057	.581		10 062	-.304	-1.448
E		.619	.00213	.471		3 959	.133	-1.524
E'		.619	.00213			3 959	.133	1.524
F		.779	.00544			30 817	-.281	1.448
G		.100	.0125	.000055		96.57	-.654	.343
H		.076	.00553	.000042		73.57	.508	0
I		.040	.00314	.0000055		9.61	-.508	0
J		.040	.00314	.0000055		9.61	0	.508
K[b]	13.5	.178	.163	0		8.05	-1.219	0
L	73.8	4.764	48.78	43.74		17.11E6	-3.188	3.347
M	73.8	.548	.00213	.295		3 747	-.136	1.270
N[c]	68.9	.320	.1086	0		51 324	-.556	0
O	73.8	1.325	3.309	.567	-.720	4 432	-1.913	-.474
P(60°)[d]		3.748	20.81	20.81	0	116 721	0	0
P(70°)[d]		.549	.716	.385	.466	818	1.508	-.582
P(90°)[d]		.345	.128	.0832	.0608	511	.836	0
P(110°)[d]		.549	.716	.385	.466	818	1.508	.582
P(180°)[d]		1.874	10.41	10.41	0	58 361	0	0

[a]Ring spacing = 5.59 - 0.0135(R - 29.5) cm.

[b]Ring spacing = 7.13 - 0.0190(R - 80) cm.

[c]Ring spacing = 12.57 cm.

[d]Longitudinal stiffeners at circumferential location indicated.

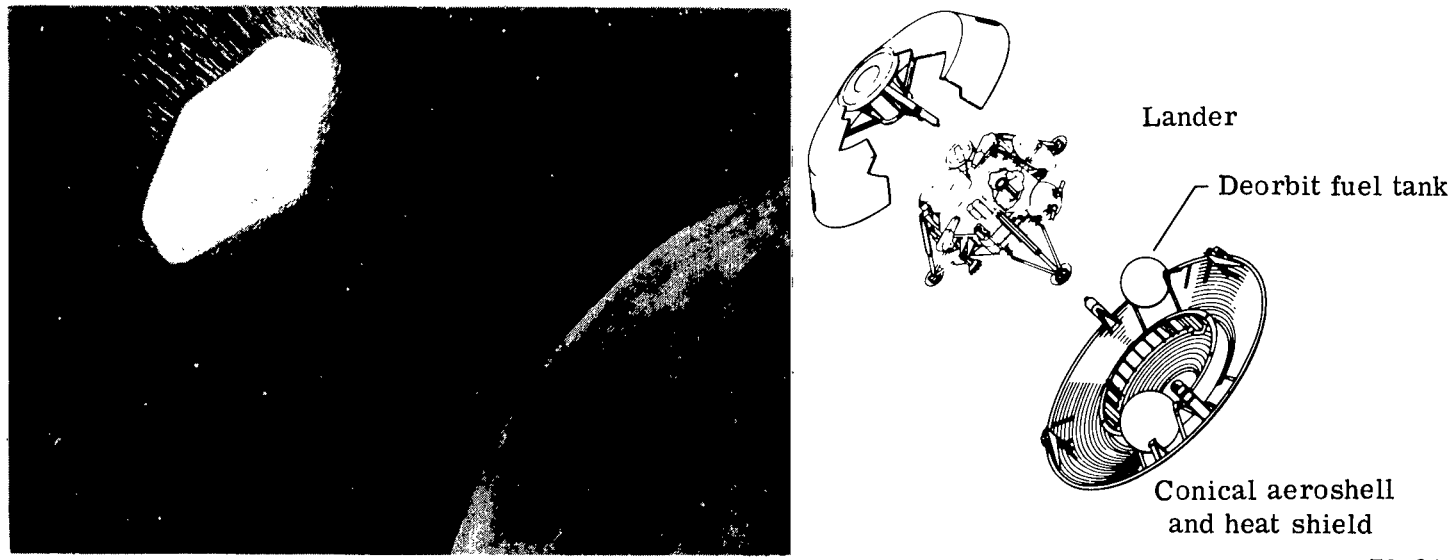

Figure 1.- Viking entry capsule.

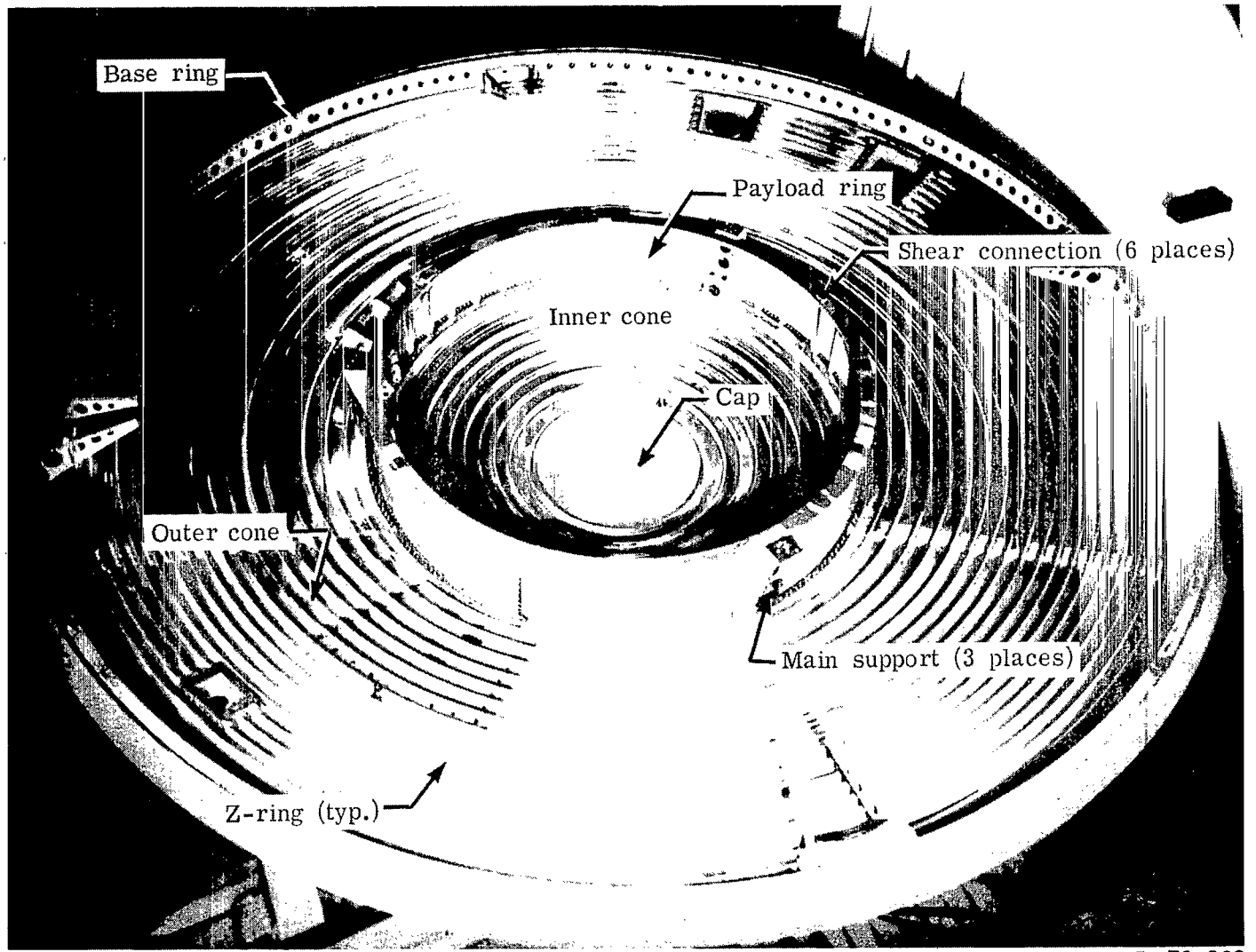

L-76-232

Figure 2.- Basic structural components of the Viking aeroshell.

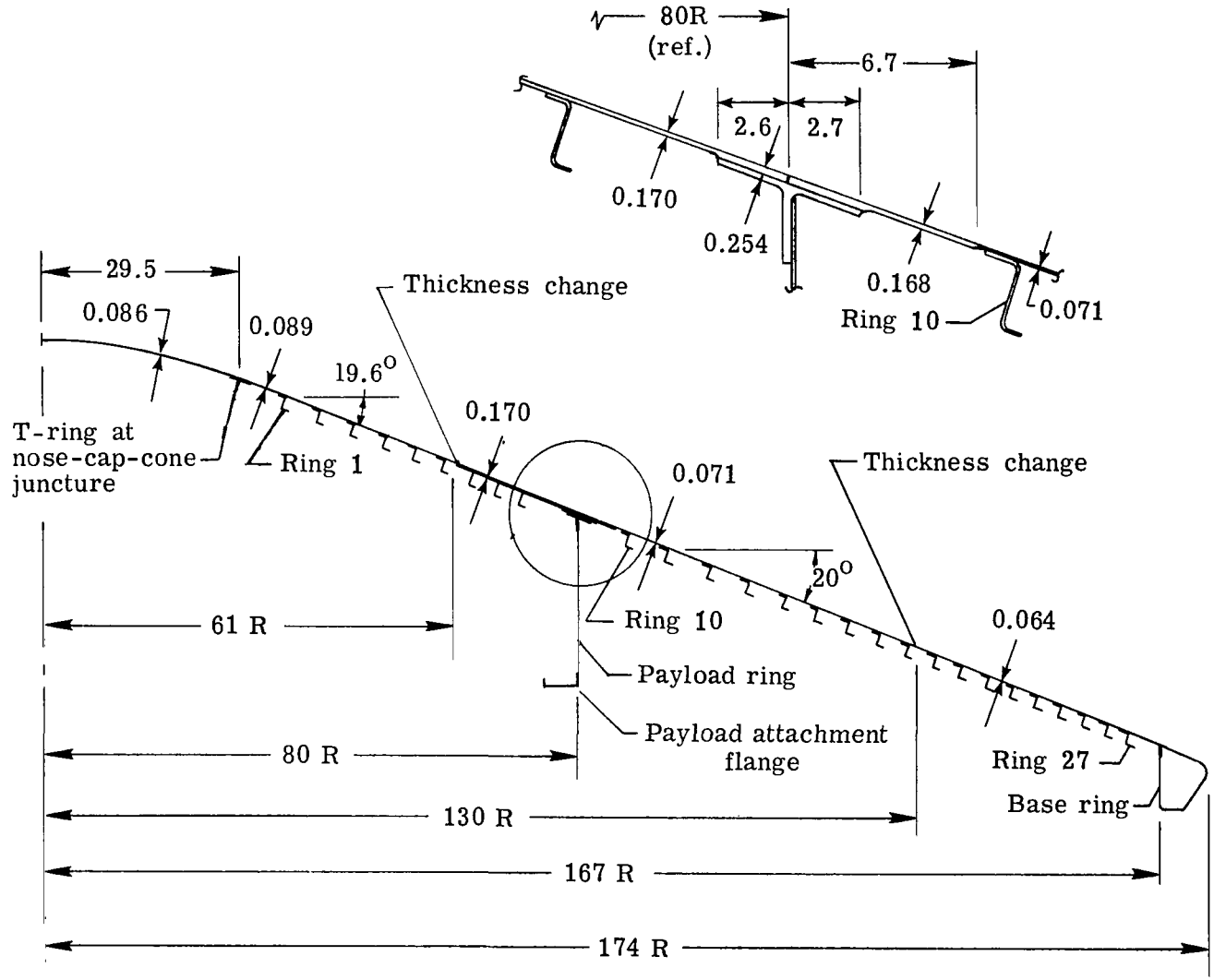

Figure 3.- Cross-sectional view of aeroshell. (Dimensions are in cm.)

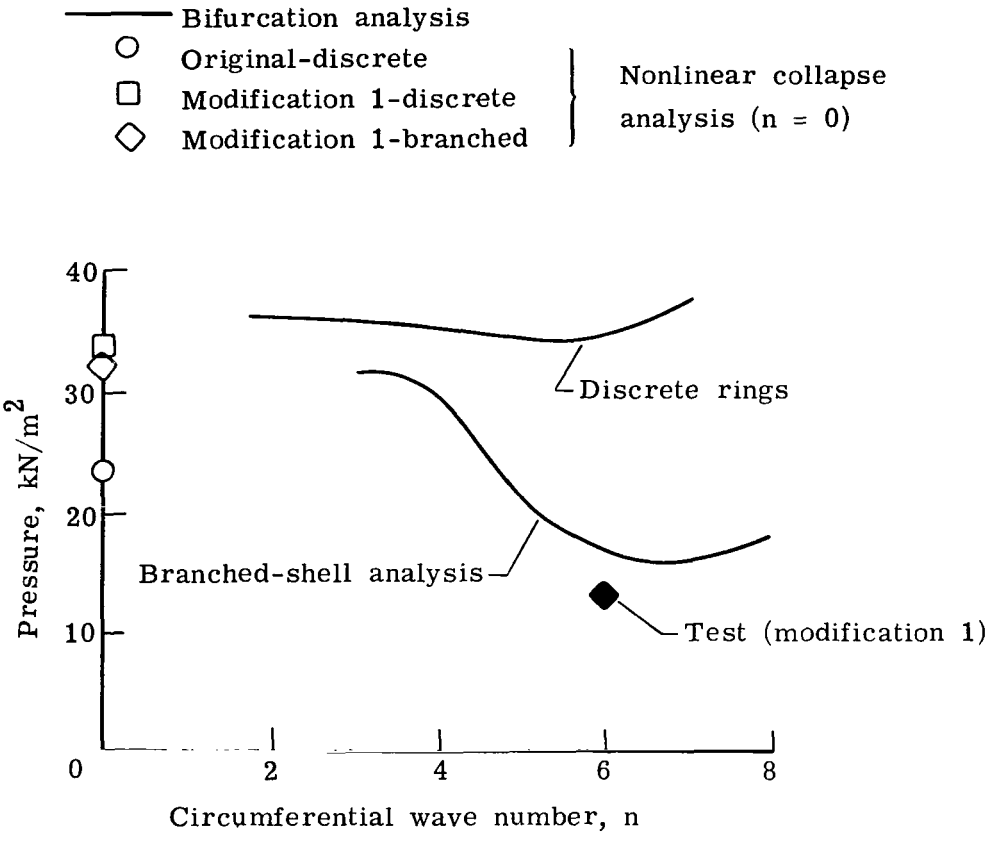

Figure 4.- Comparison of analytical results with experiment for aeroshell with first modification.

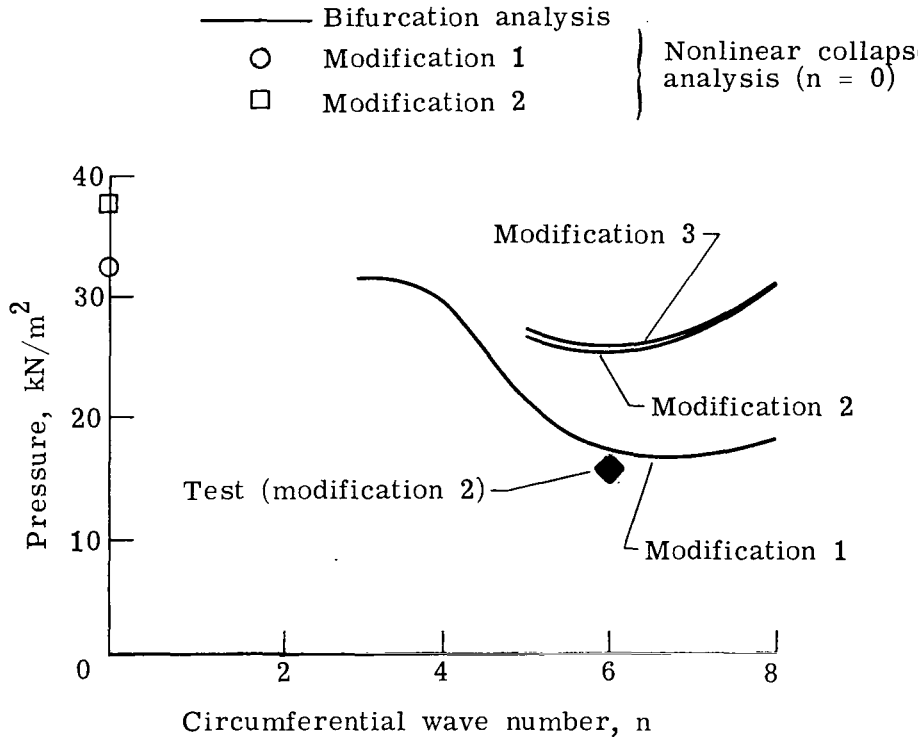

Figure 5.- Effect of aeroshell modifications on analytical buckling strength. Branched model used for all analyses.

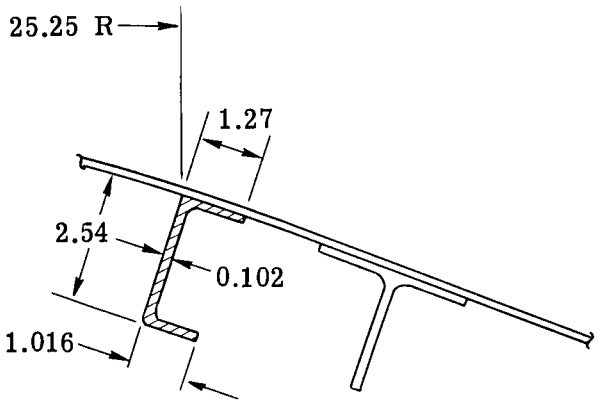

Detail A

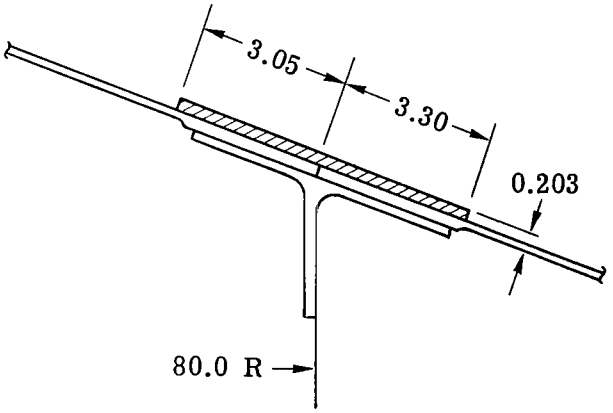

Detail B

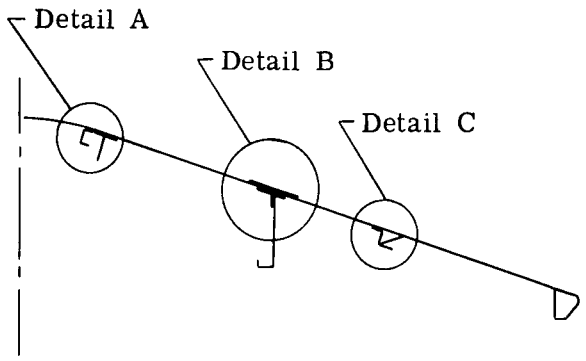

Aeroshell

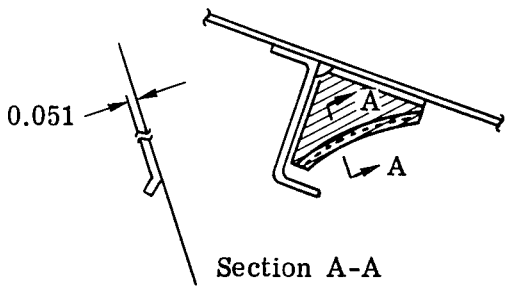

Section A-A

Detail C

Figure 6.- Details of aeroshell structural modification 3. (Dimensions are in cm.)

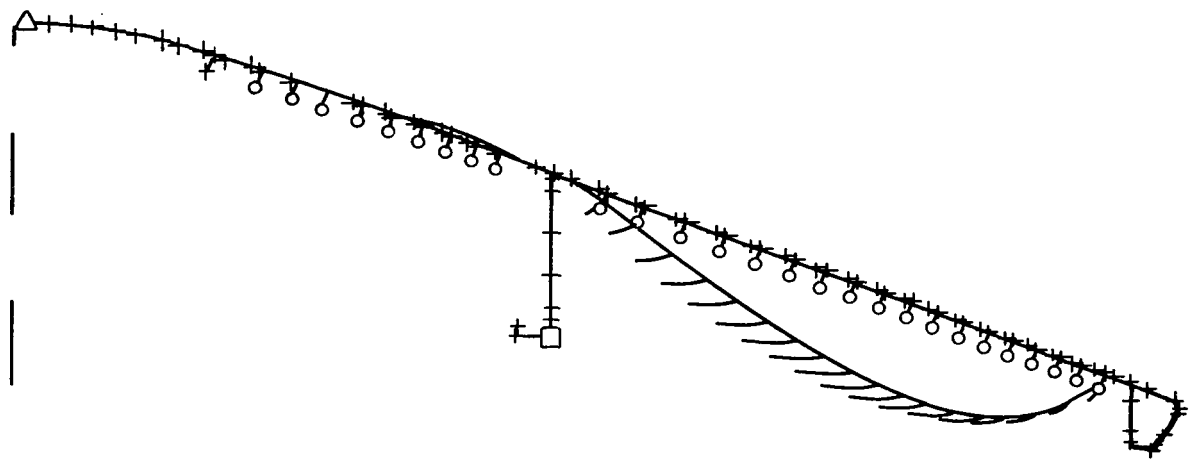

(a) n = 7 mode for aeroshell with modification 1.

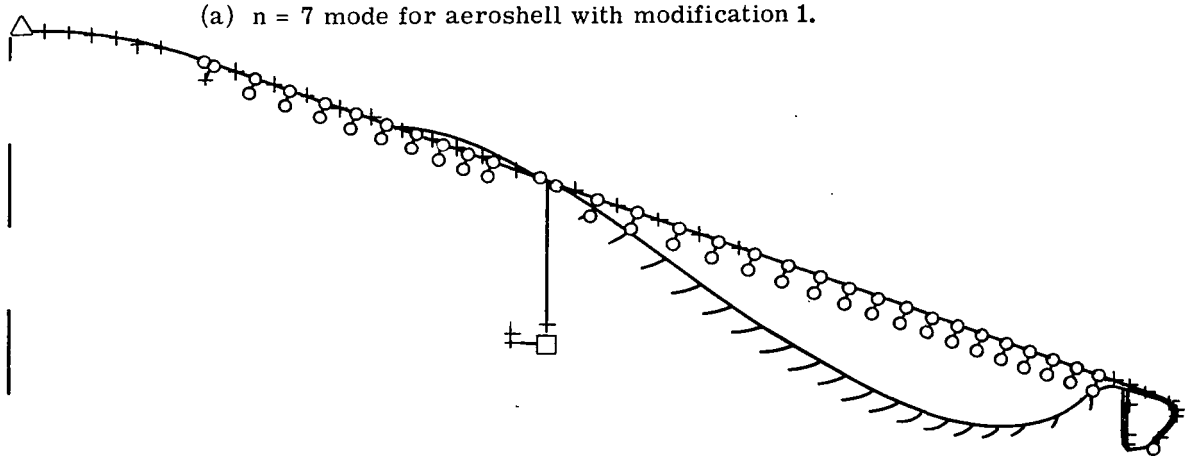

(b) n = 6 mode for aeroshell with modification 2.

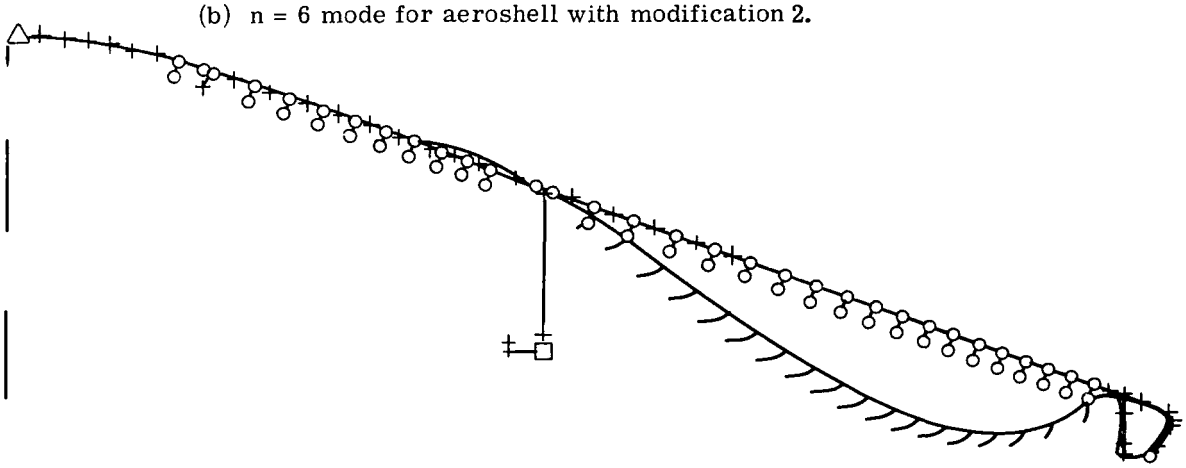

(c) n = 6 mode for aeroshell with modification 3.

Figure 7.- Critical buckling mode shapes for various models of the Viking aeroshell.

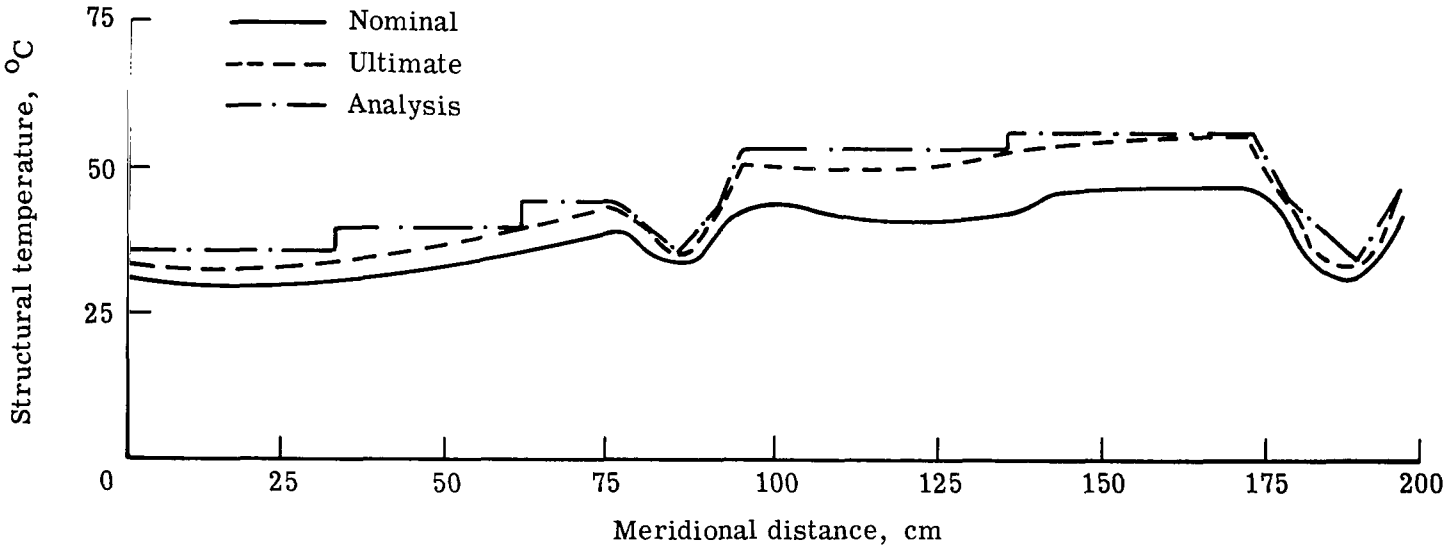

Figure 8.- Aeroshell structural temperatures at maximum dynamic pressure as a function of meridional distance.

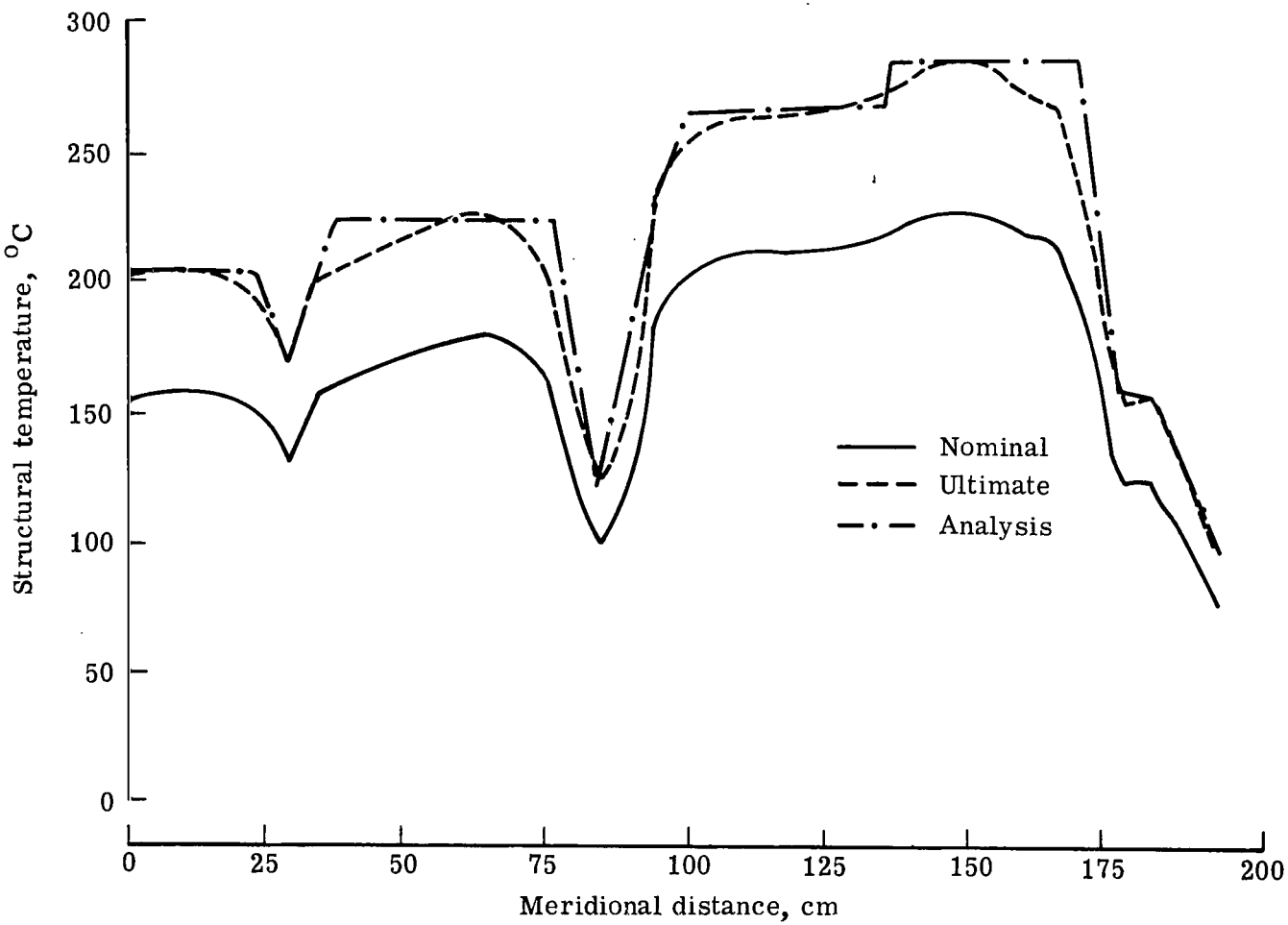

Figure 9.- Maximum aeroshell structural temperatures as a function of meridional distance.

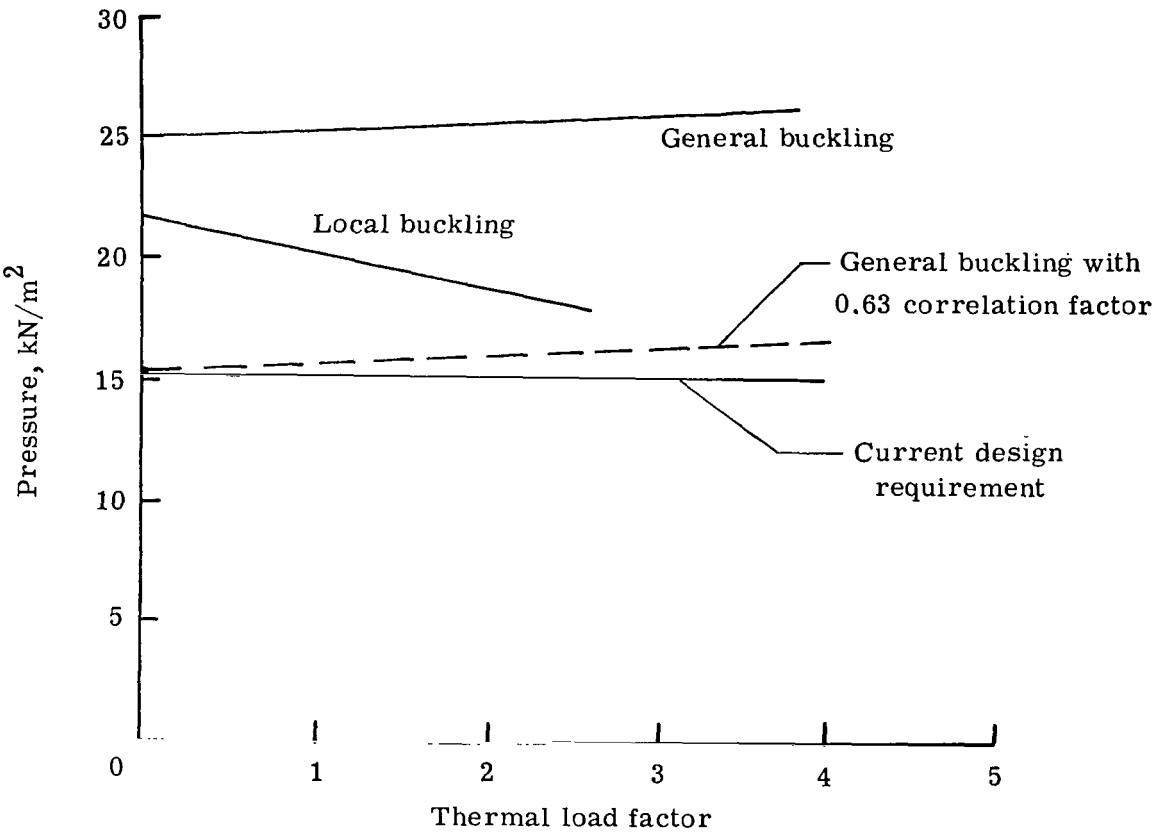

Figure 10.- Interaction curves for buckling strength as a function of both normal external pressure and structural temperatures at maximum dynamic pressure.

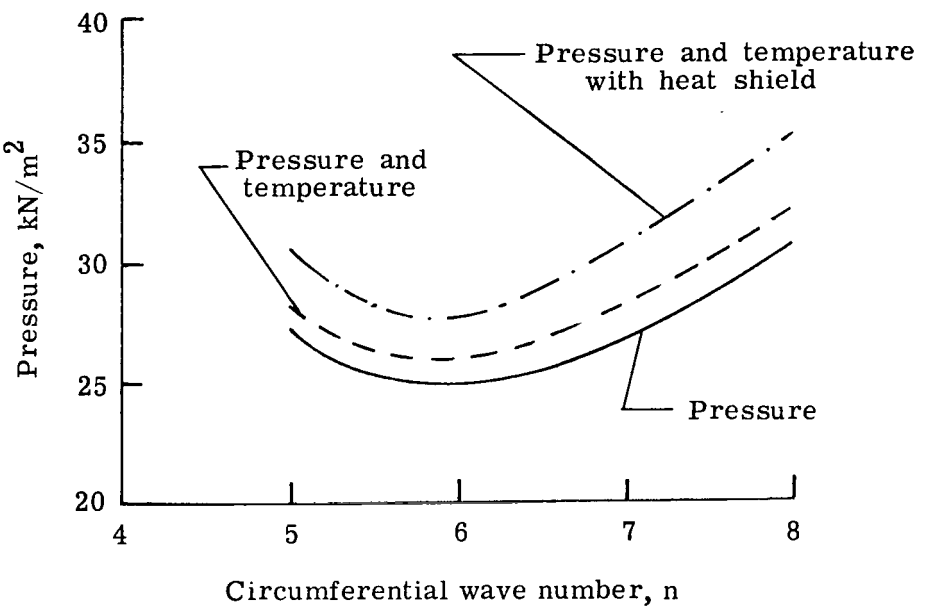

Figure 11.- Effects of temperature and heat-shield properties at maximum dynamic pressure on buckling strength for the aeroshell with modification 3.

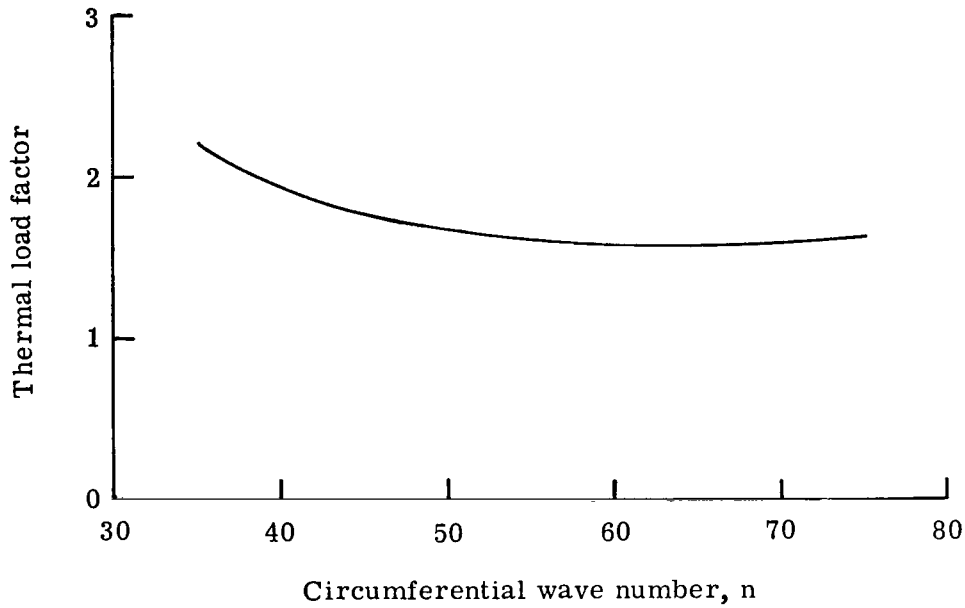

Figure 12.- Local buckling strength as a function of circumferential wavelength for a segment of the aeroshell at maximum temperature.

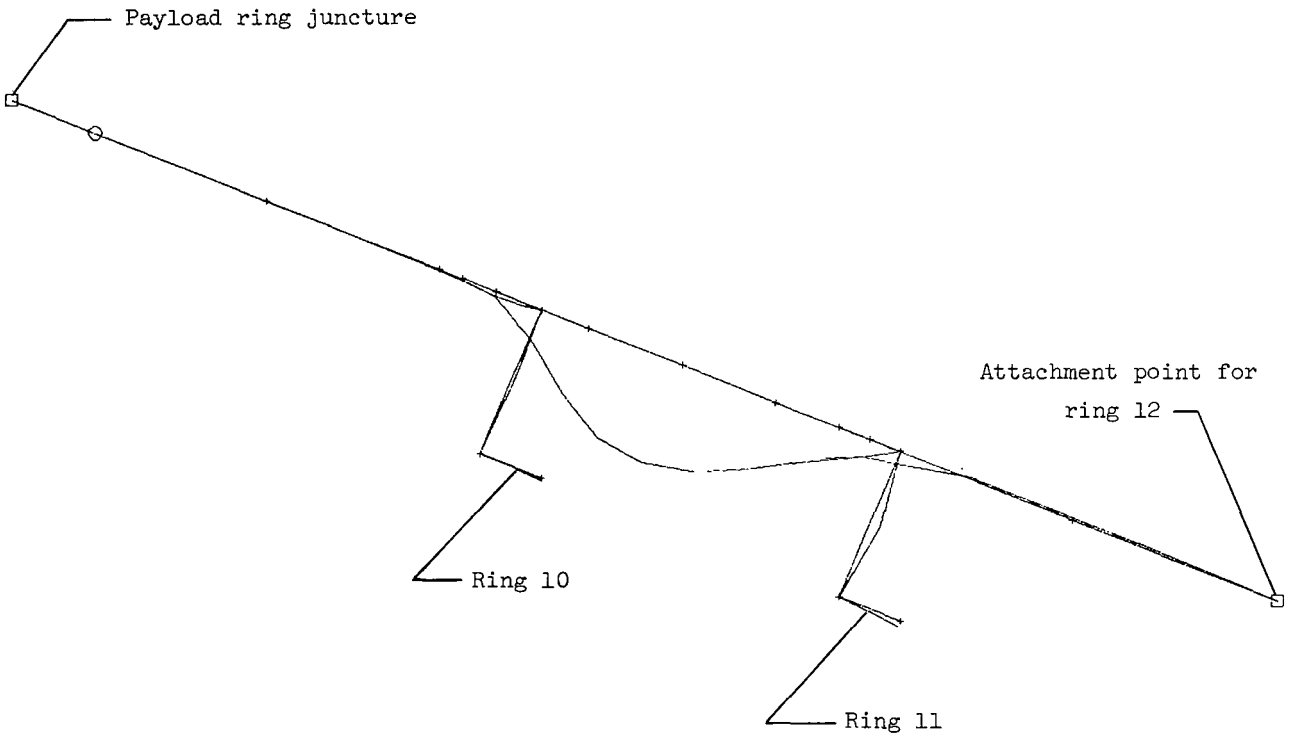

Figure 13.- Critical buckling mode shape at n = 65 for a segment of the aeroshell loaded with maximum temperature. (Thermal multiplier = 1.59.)

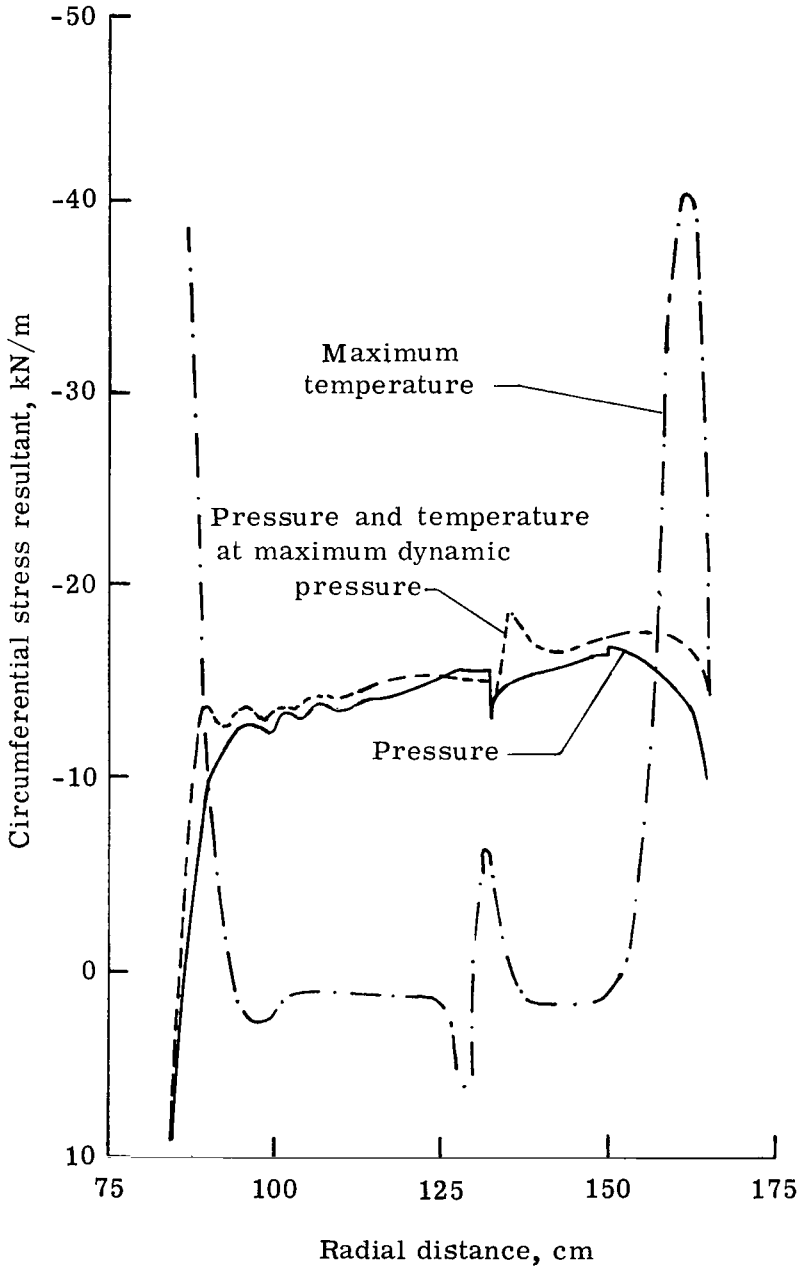

Figure 14.- Comparison of stress states under various load conditions.

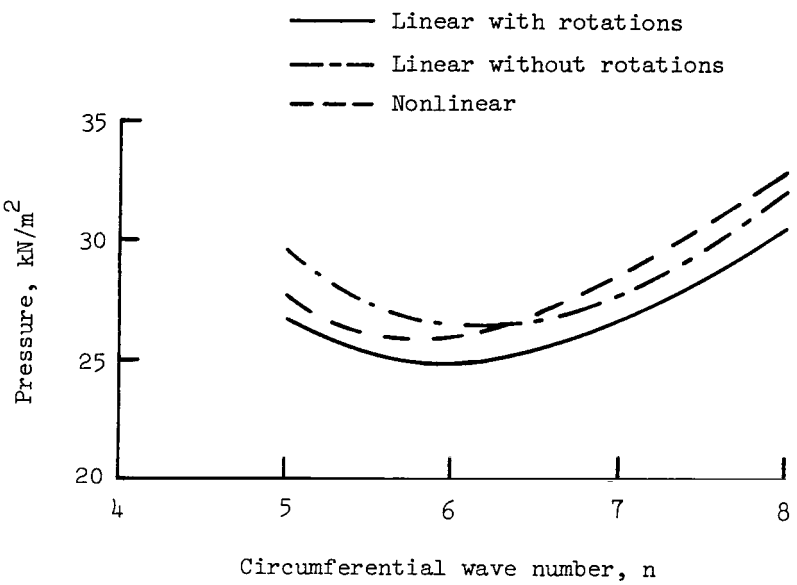

Figure 15.- Effect of including geometric nonlinearities and rotations in buckling analysis.

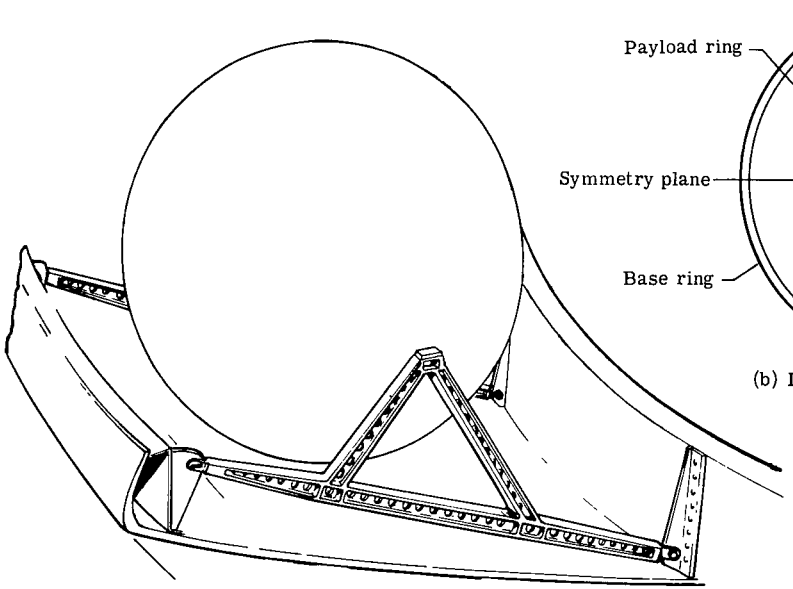

(a) Deorbit fuel tank and truss.

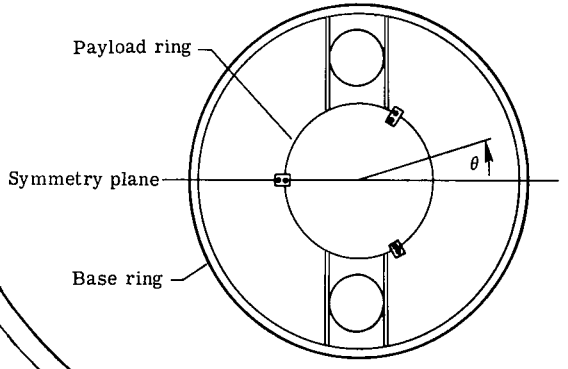

(b) Deorbit fuel-tank locations.

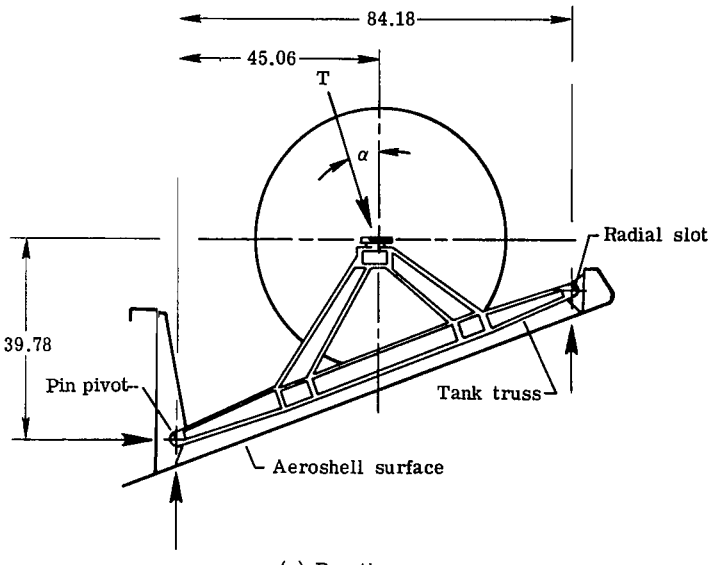

(c) Reactions.

Figure 16.- Deorbit fuel-tank locations and truss attachments. (Dimensions are in cm.)

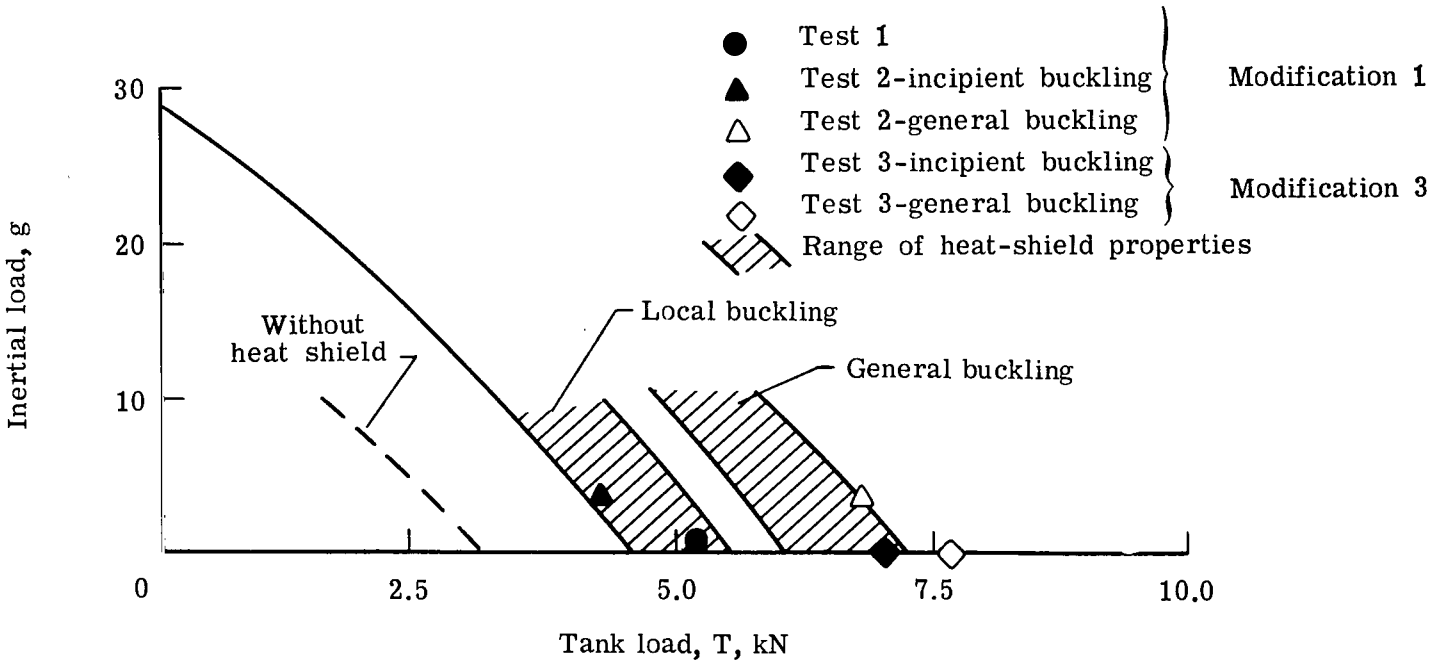

Figure 17.- Comparison of experimental results with analytical interaction curves for inertial and tank loads.

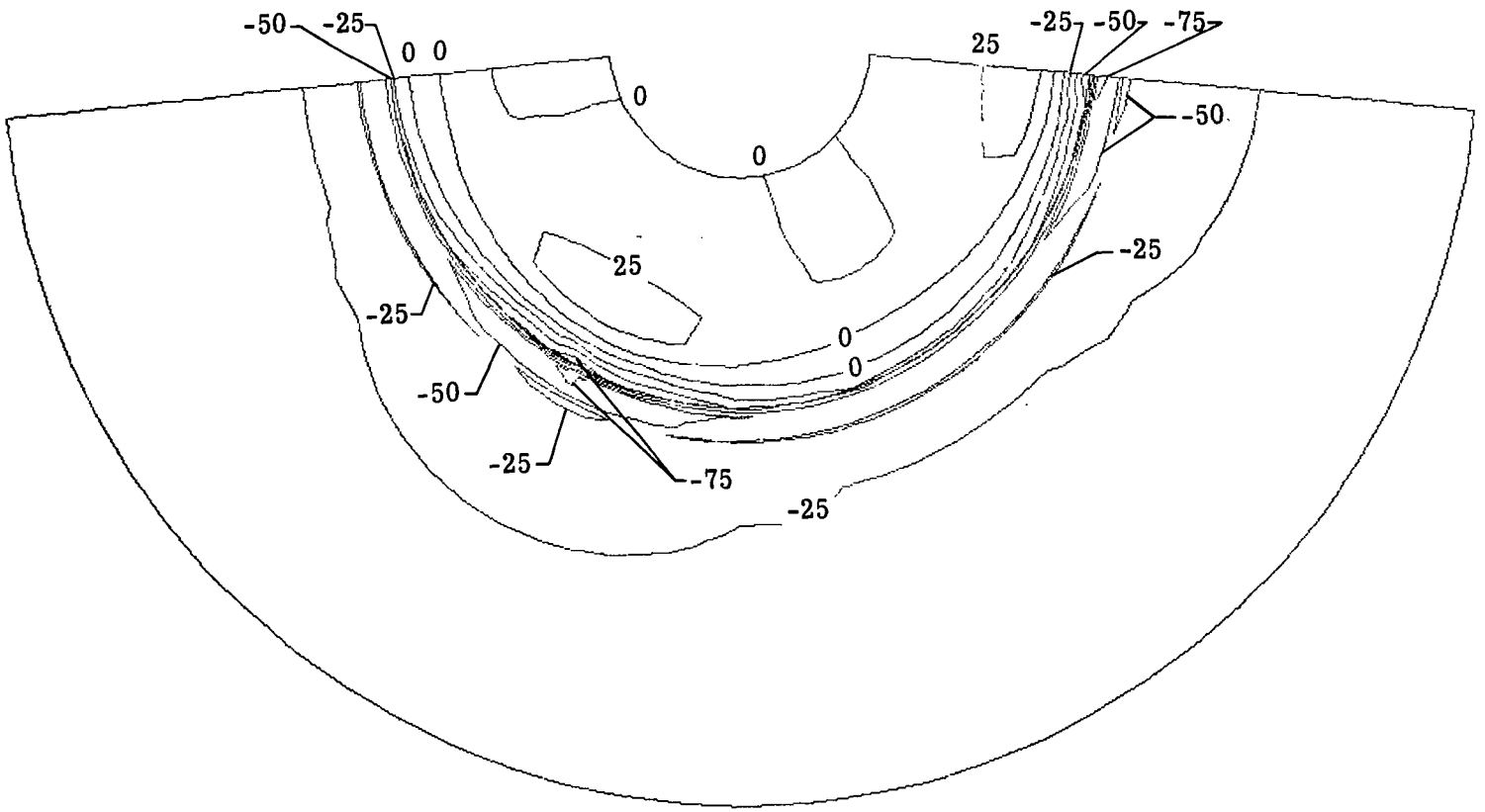

(a) 1g inertial load, $N_{x_{max}} = 7.285$ kN/m.

Figure 18.- Contour plots for meridional stress resultants on developed surface of conical aeroshell. Contours are percentages of maximum value of the meridional stress resultant, N_x.

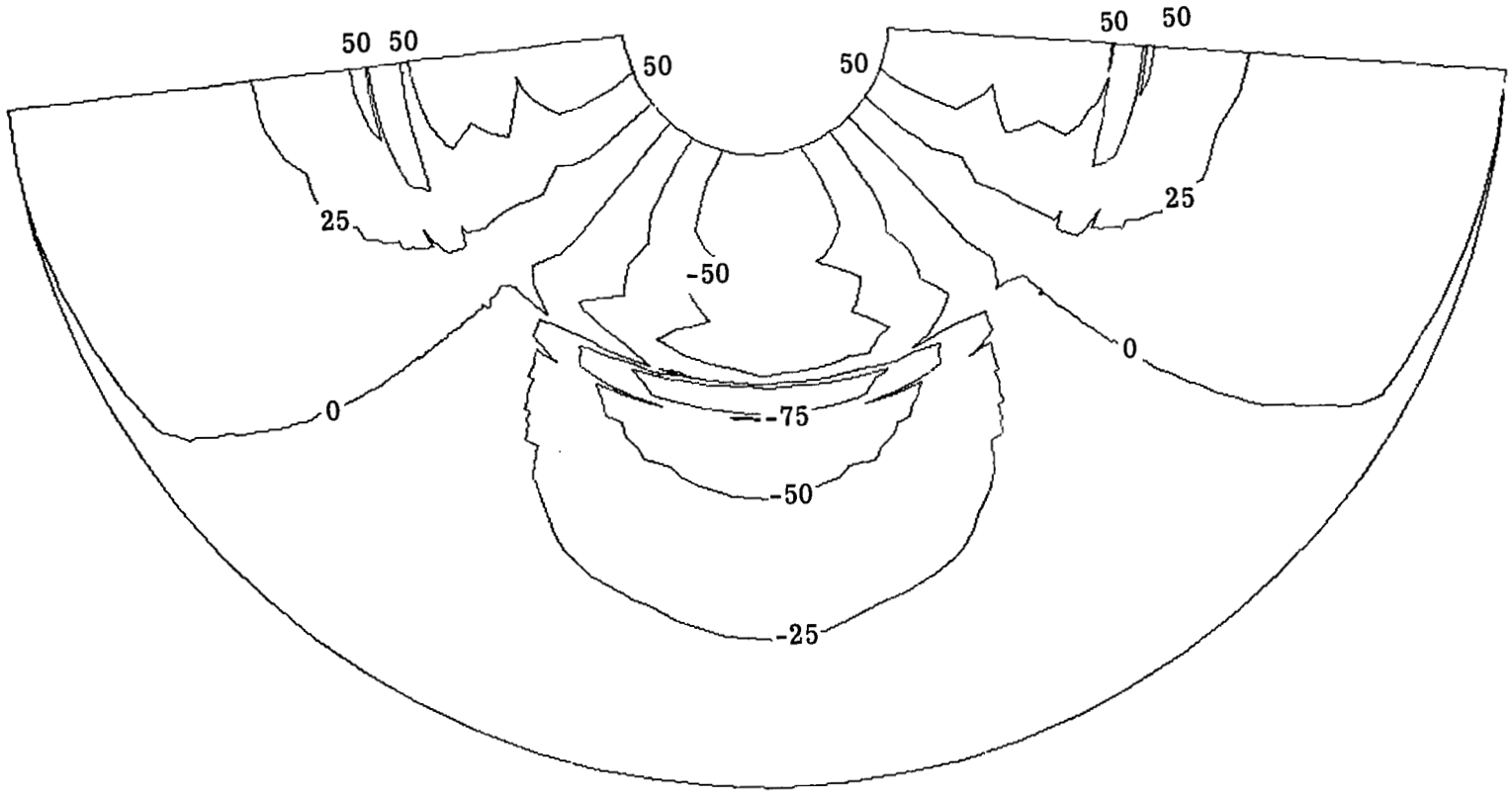

(b) Unit tank load, $N_{x_{max}} = 26.6$ N/m.

Figure 18.- Concluded.

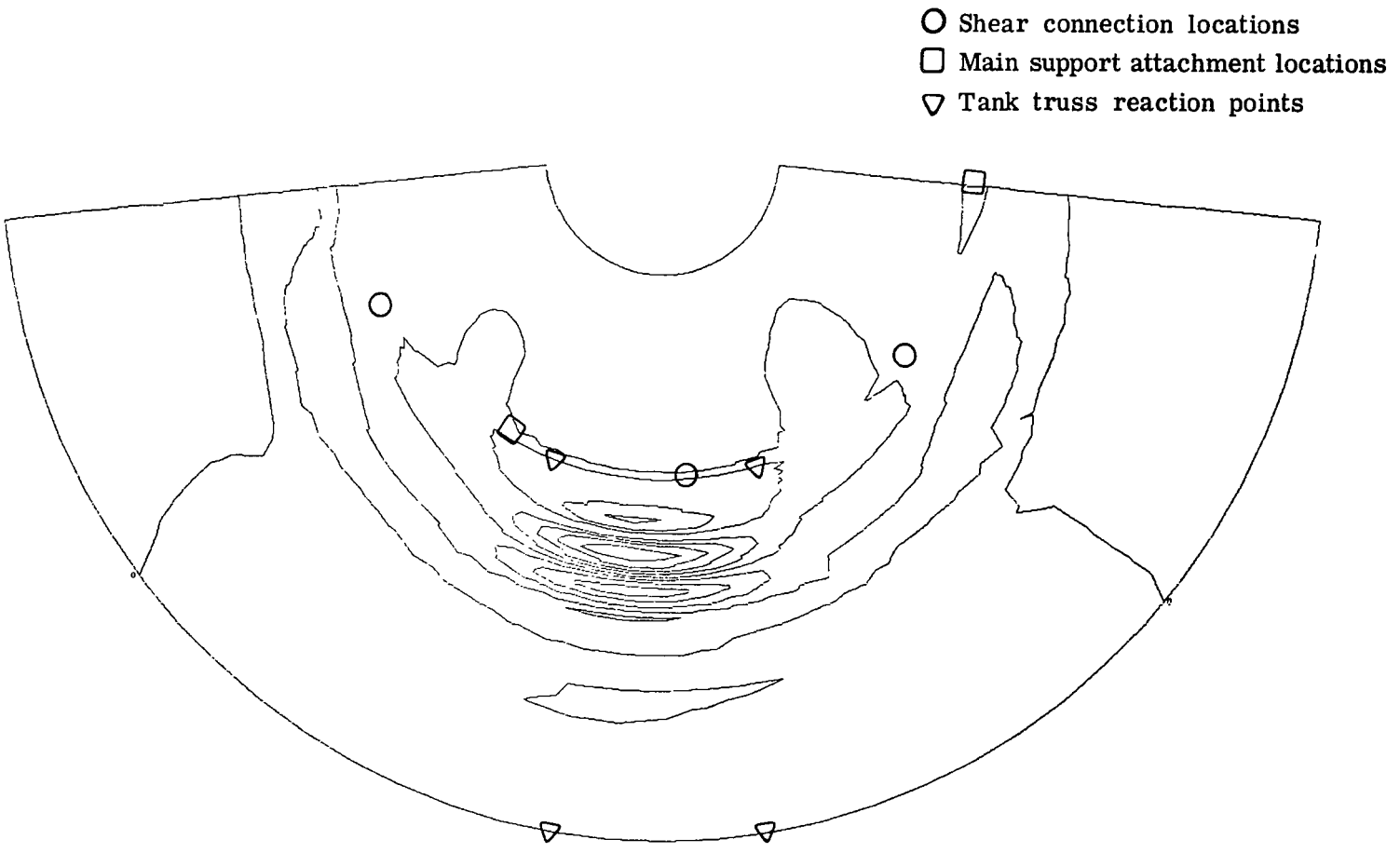

Figure 19.- Buckling contour plot on a developed surface for a mode shape of normal displacement at a 4.56g load and a 4.30 kN tank load.

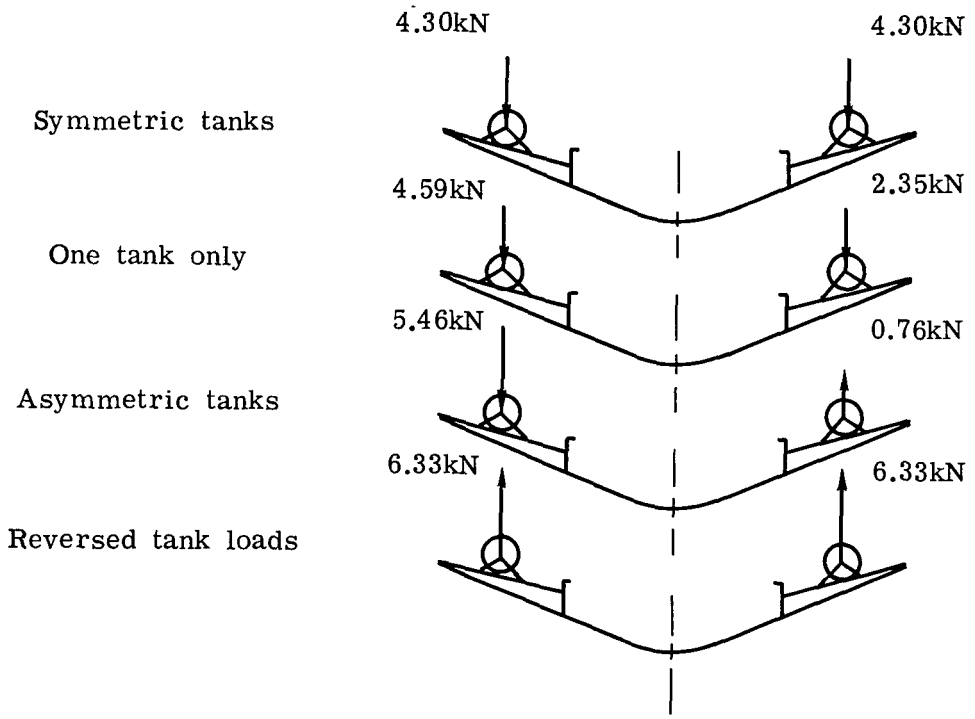

Figure 20.- Load combinations possible at base ring during pogo. All loads include 4.56g tank-load steady-state component on base ring.

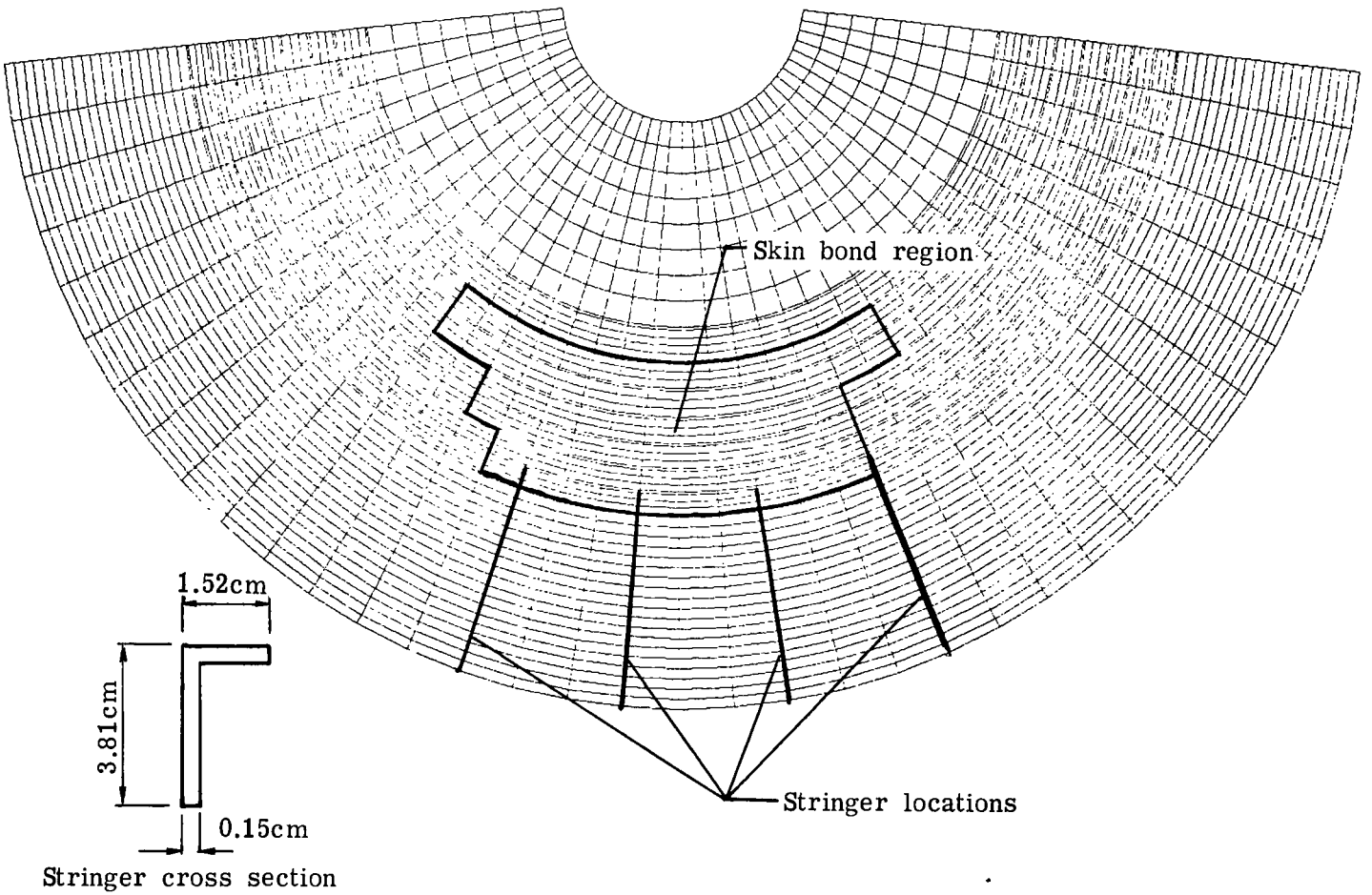

Figure 21.- Skin bonding and stringer reinforcement concept for local strengthening of aeroshell displayed on developed surface.

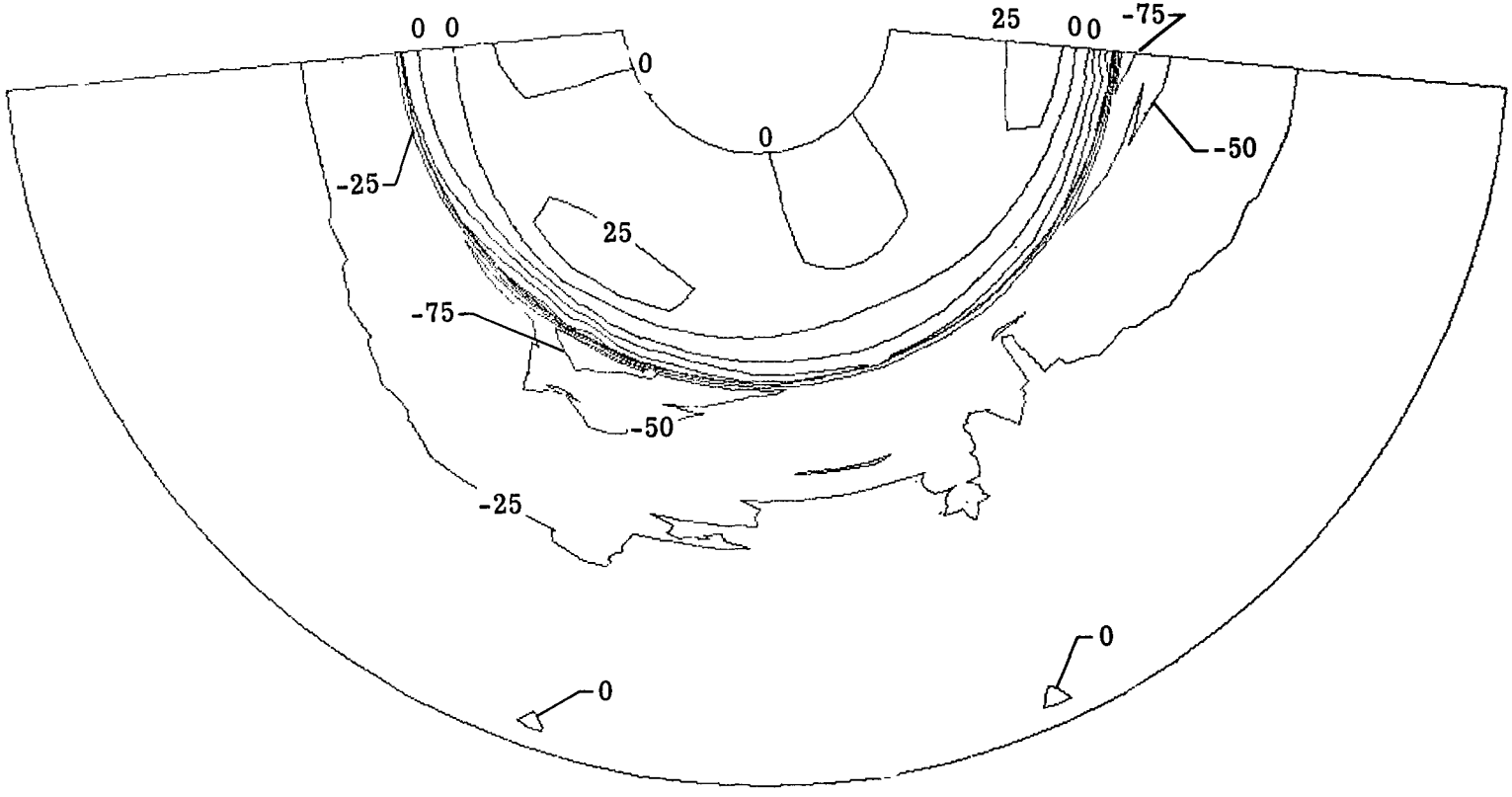

(a) 1g inertial load, $N_{x_{max}} = 6.429$ kN/m.

Figure 22.- Contour plots for meridional stress resultants on developed surface of conical aeroshell with local skin band and stringer reinforcement. Contours are percentages of maximum value of the meridional stress resultant, N_x.

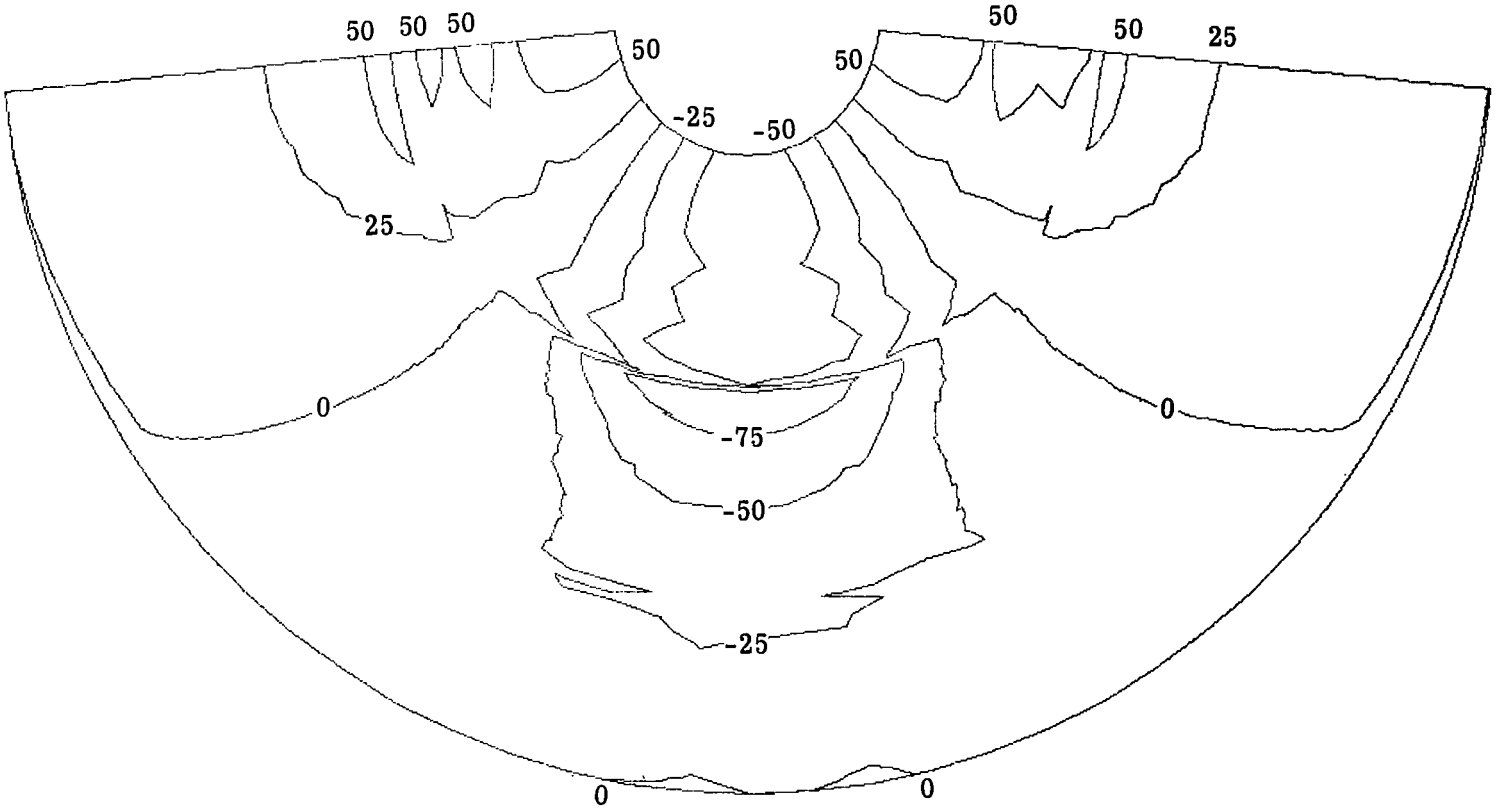

(b) Unit tank load, $N_{x_{max}} = 28.9$ N/m.

Figure 22.- Concluded.

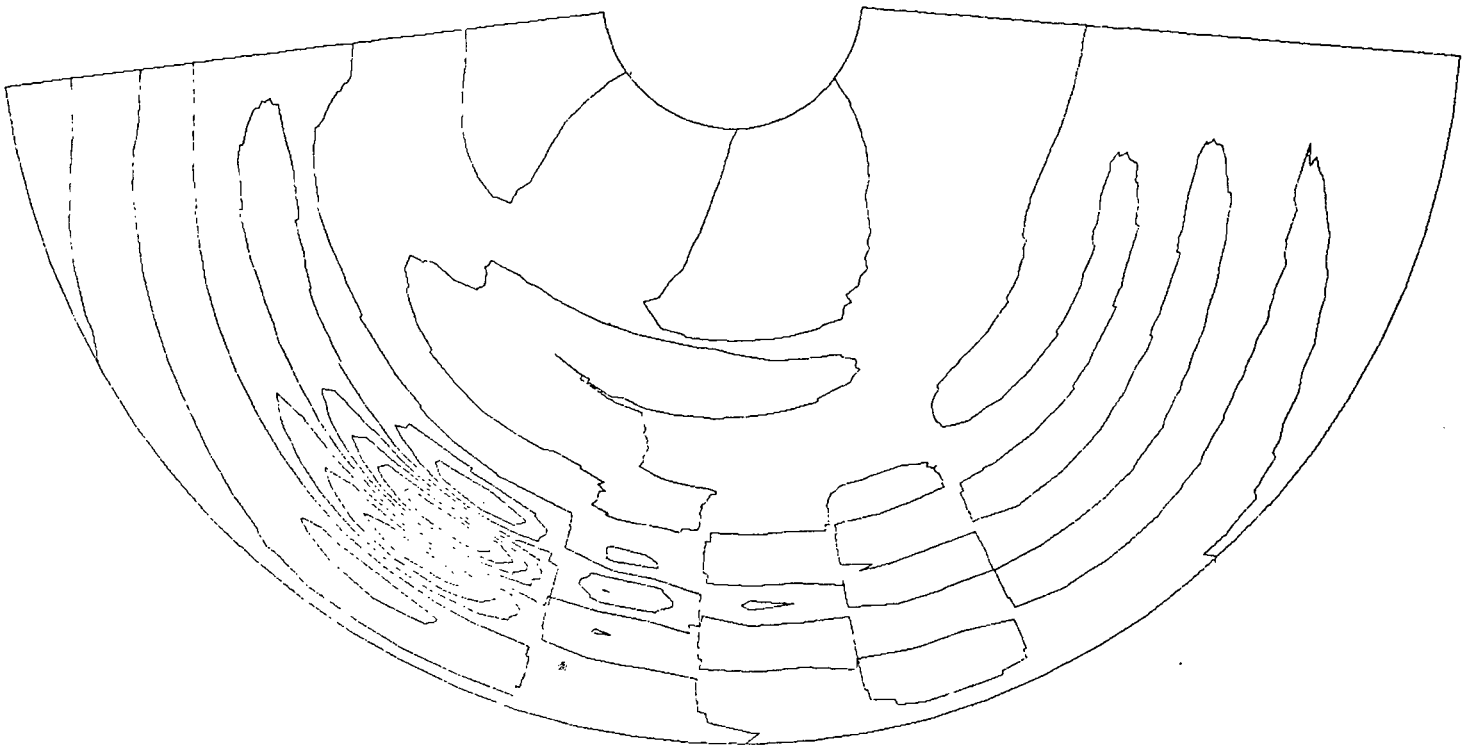

Figure 23.- Contour plot of buckling mode for normal displacement on developed surface of aeroshell with skin bond and stringer reinforcements.

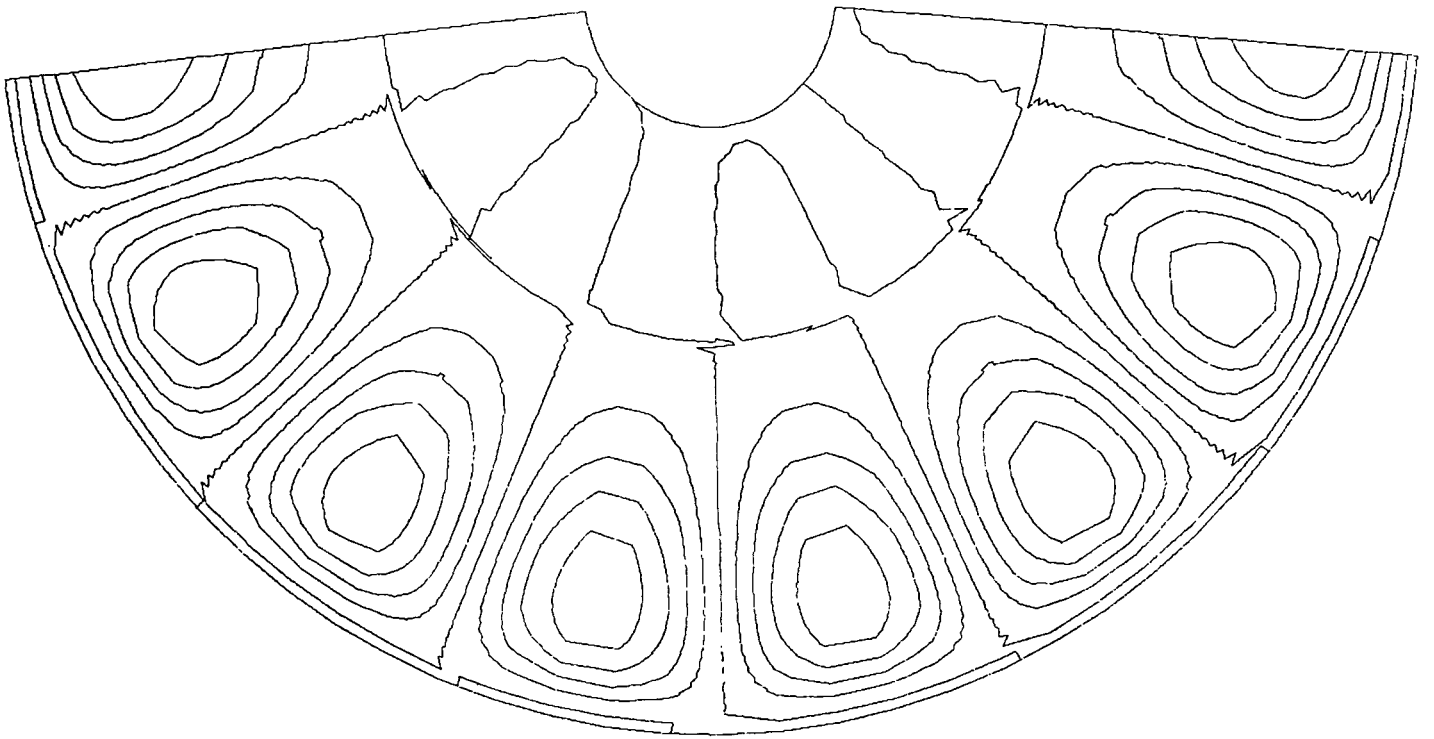

(a) Aeroshell.

Figure 24.- Contour plots on developed conical shell surface for buckling mode shape of normal displacement due to external pressure.

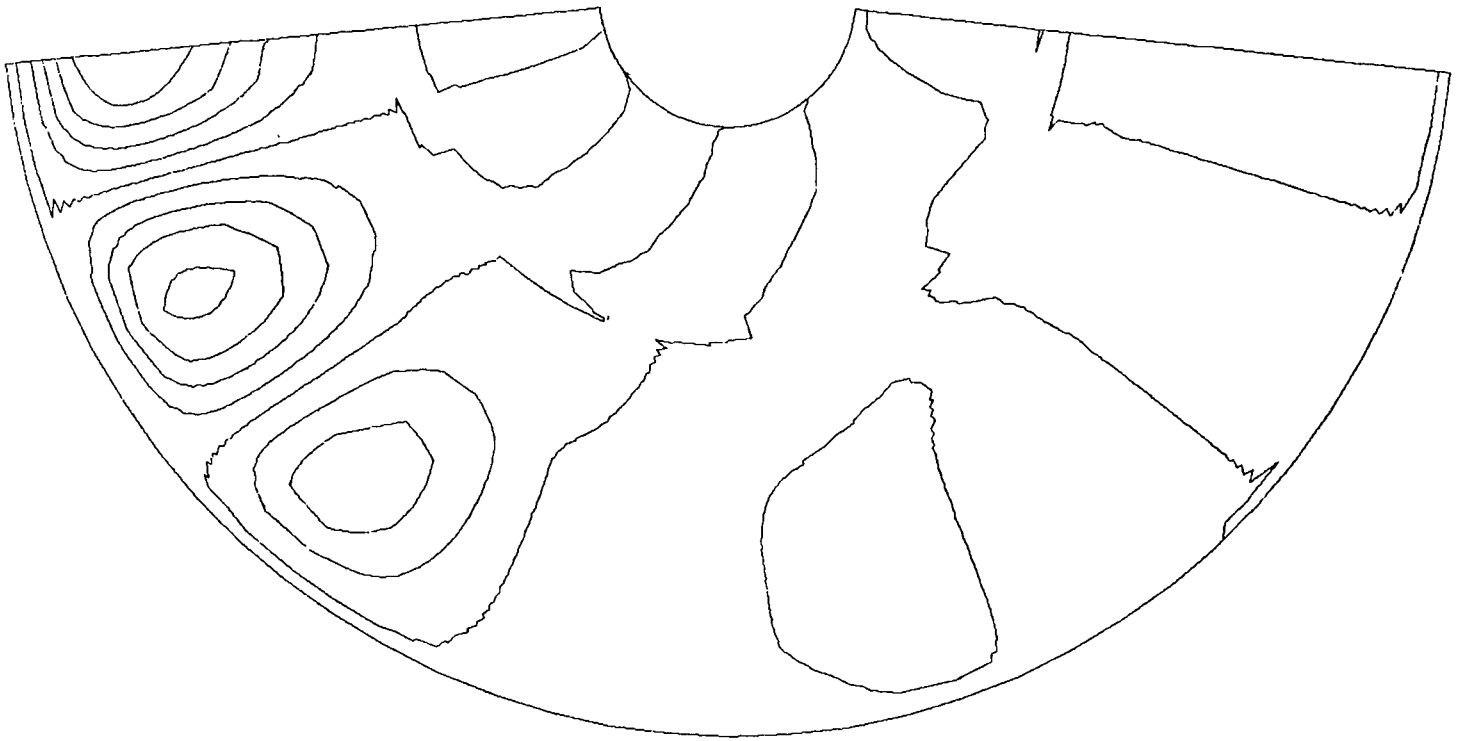

(b) Aeroshell with local reinforcement.

Figure 24. - Concluded.

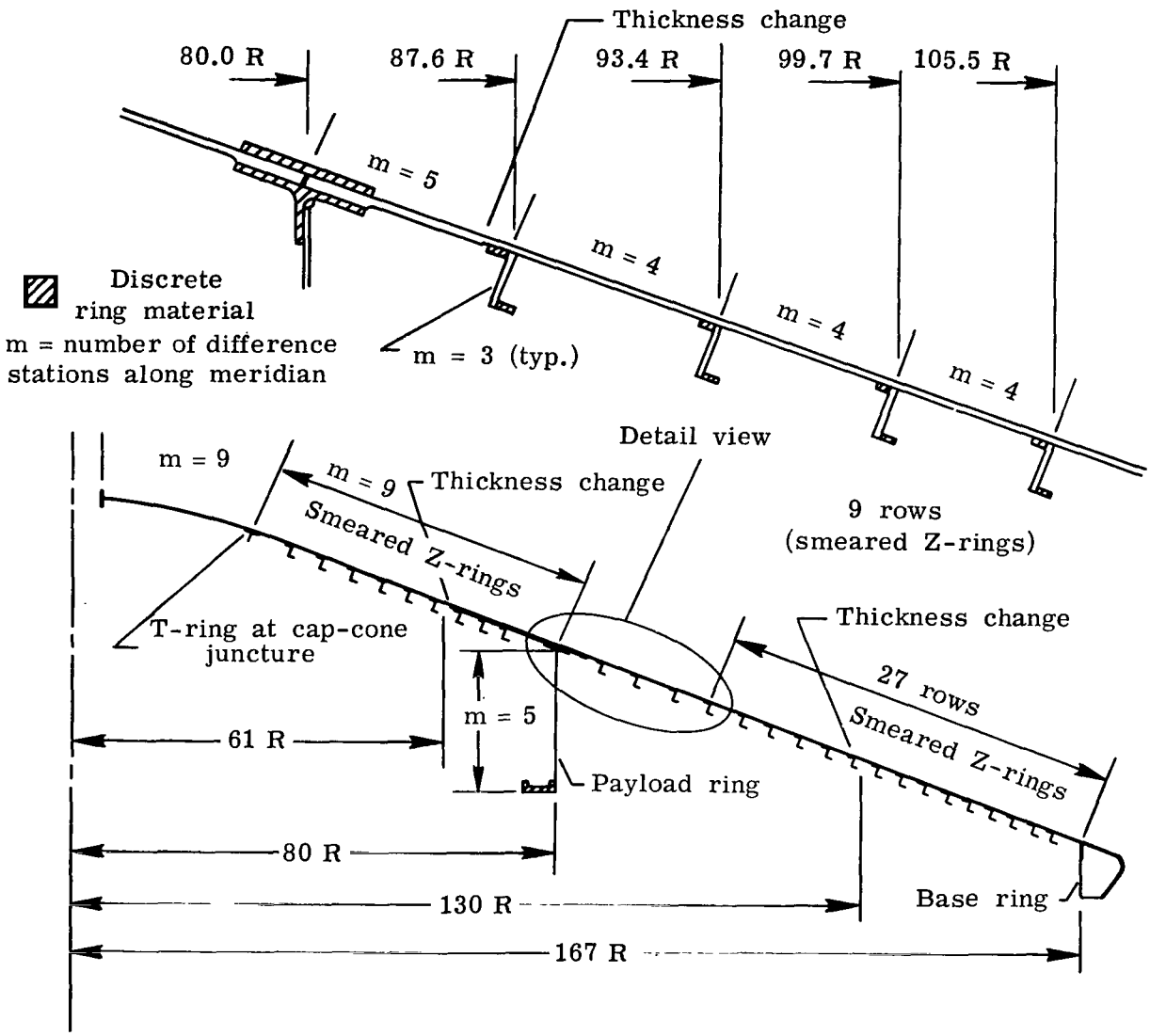

Figure 25.- Details of STAGS model for the aeroshell with modification 1.
(Dimensions are in cm.)

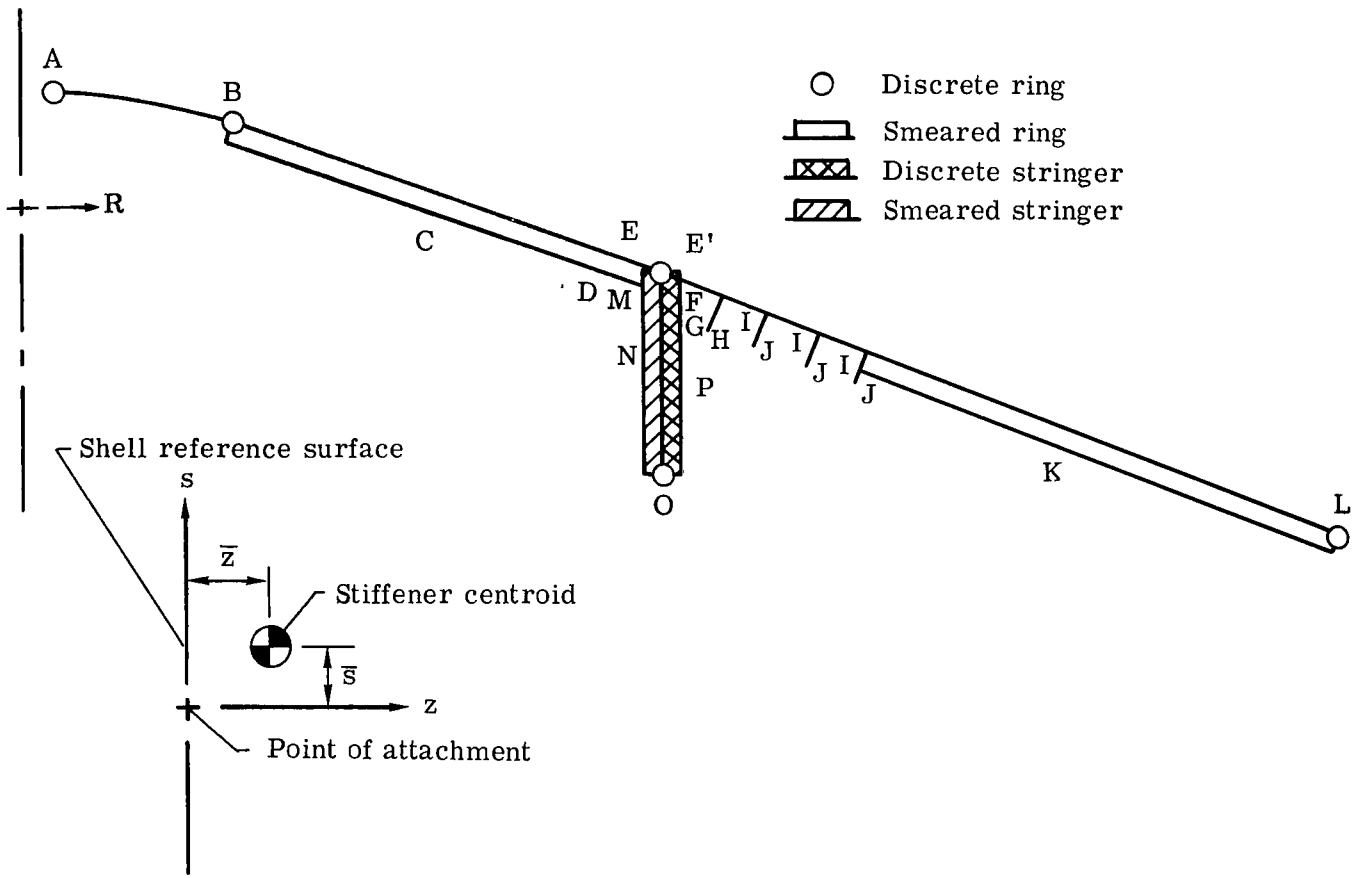

Figure 26.- Key to locations of discrete and smeared stiffener properties tabulated in table L

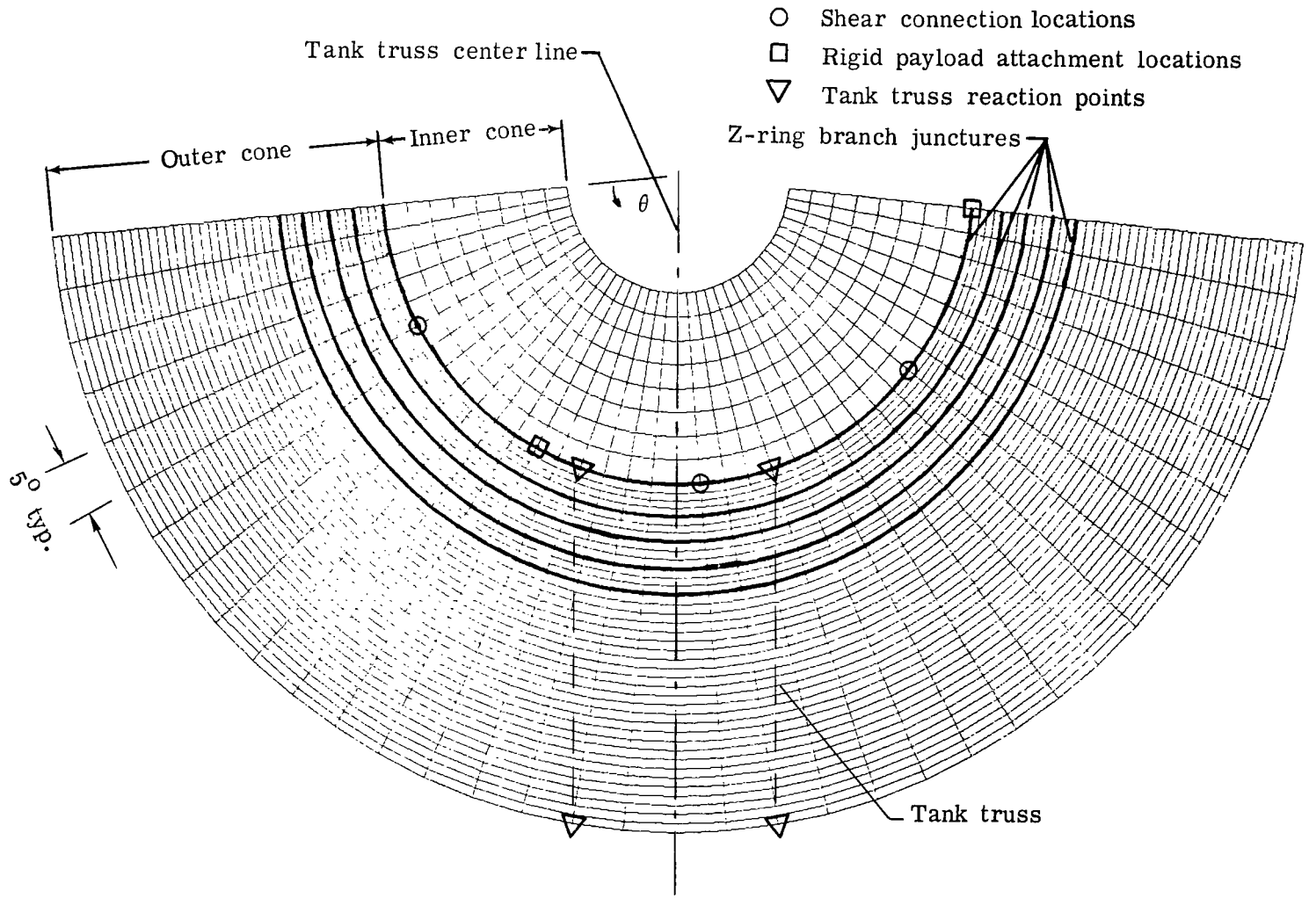

Figure 27.- Developed view of 180° STAGS model for inner and outer cone-surface finite-difference grid.

Figure 28.- Distributed and concentrated loads comprising a 1g inertial load (without the fuel-tank loads) for the STAGS aeroshell model. All loads shown are in the positive z direction.

NASA-Langley, 1976 L-10751

"The aeronautical and space activities of the United States shall be conducted so as to contribute . . . to the expansion of human knowledge of phenomena in the atmosphere and space. The Administration shall provide for the widest practicable and appropriate dissemination of information concerning its activities and the results thereof."

—NATIONAL AERONAUTICS AND SPACE ACT OF 1958

NASA SCIENTIFIC AND TECHNICAL PUBLICATIONS

TECHNICAL REPORTS: Scientific and technical information considered important, complete, and a lasting contribution to existing knowledge.

TECHNICAL NOTES: Information less broad in scope but nevertheless of importance as a contribution to existing knowledge.

TECHNICAL MEMORANDUMS: Information receiving limited distribution because of preliminary data, security classification, or other reasons. Also includes conference proceedings with either limited or unlimited distribution.

CONTRACTOR REPORTS: Scientific and technical information generated under a NASA contract or grant and considered an important contribution to existing knowledge.

TECHNICAL TRANSLATIONS: Information published in a foreign language considered to merit NASA distribution in English.

SPECIAL PUBLICATIONS: Information derived from or of value to NASA activities. Publications include final reports of major projects, monographs, data compilations, handbooks, sourcebooks, and special bibliographies.

TECHNOLOGY UTILIZATION PUBLICATIONS: Information on technology used by NASA that may be of particular interest in commercial and other non-aerospace applications. Publications include Tech Briefs, Technology Utilization Reports and Technology Surveys.

Details on the availability of these publications may be obtained from:

SCIENTIFIC AND TECHNICAL INFORMATION OFFICE

NATIONAL AERONAUTICS AND SPACE ADMINISTRATION

Washington, D.C. 20546